Montclair State University
Montclair State University Digital Commons

Department of Earth and Environmental Studies Faculty Scholarship and Creative Works

Department of Earth and Environmental Studies

6-28-2012

Chronostratigraphic Framework for the IODP Expedition 318 Cores from the Wilkes Land Margin: Constraints for Paleoceanographic Reconstruction

Lisa Tauxe
Scripps Institute of Oceanography, ltauxe@ucsd.edu

Catherine E. Stickley
University of Tromsø

Saiko Sugisaki
Science University of Tokyo in Yamaguchi

Peter K. Bijl
Utrecht University

Steven M. Bohaty
University of Southampton

See last page for additional authors

Follow this and additional works at: https://digitalcommons.montclair.edu/earth-environ-studies-facpubs

Part of the Geology Commons, and the Stratigraphy Commons

MSU Digital Commons Citation

Tauxe, Lisa; Stickley, Catherine E.; Sugisaki, Saiko; Bijl, Peter K.; Bohaty, Steven M.; Brinkhuis, Henk; Escutia, Carlota; Flores, J. A.; Houben, A. J. P.; Iwai, M.; Jiménez-Espejo, Francisco J.; McKay, Robert; Passchier, Sandra; Pross, Jörg; Riesselman, Christina; Röhl, Ursula; Sangiorgi, Francesca; Welsh, Kevin; Klaus, Adam; Fehr, Annick; Bendle, James; Dunbar, Robert B.; Gonzàlez, J.; Hayden, T.; Katsuki, K.; Olney, M. P.; Pekar, Stephen; Shrivastava, P. K.; van de Flierdt, Tina; Williams, Trevor; and Yamane, M., "Chronostratigraphic Framework for the IODP Expedition 318 Cores from the Wilkes Land Margin: Constraints for Paleoceanographic Reconstruction" (2012). *Department of Earth and Environmental Studies Faculty Scholarship and Creative Works*. 43.
https://digitalcommons.montclair.edu/earth-environ-studies-facpubs/43

Published Citation

Tauxe, L., Stickley, C. E., Sugisaki, S., Bijl, P. K., Bohaty, S. M., Brinkhuis, H., . . . Yamane, M. (2012). Chronostratigraphic framework for the IODP Expedition 318 cores from the Wilkes Land Margin: Constraints for paleoceanographic reconstruction. Paleoceanography, 27. doi:10.1029/2012PA002308

Authors
Lisa Tauxe, Catherine E. Stickley, Saiko Sugisaki, Peter K. Bijl, Steven M. Bohaty, Henk Brinkhuis, Carlota Escutia, J. A. Flores, A. J. P. Houben, M. Iwai, Francisco J. Jiménez-Espejo, Robert McKay, Sandra Passchier, Jörg Pross, Christina Riesselman, Ursula Röhl, Francesca Sangiorgi, Kevin Welsh, Adam Klaus, Annick Fehr, James Bendle, Robert B. Dunbar, J. Gonzàlez, T. Hayden, K. Katsuki, M. P. Olney, Stephen Pekar, P. K. Shrivastava, Tina van de Flierdt, Trevor Williams, and M. Yamane

This article is available at Montclair State University Digital Commons: https://digitalcommons.montclair.edu/earth-environ-studies-facpubs/43

Chronostratigraphic framework for the IODP Expedition 318 cores from the Wilkes Land Margin: Constraints for paleoceanographic reconstruction

L. Tauxe,[1] C. E. Stickley,[2] S. Sugisaki,[1] P. K. Bijl,[3] S. M. Bohaty,[4] H. Brinkhuis,[3] C. Escutia,[5] J. A. Flores,[6] A. J. P. Houben,[3] M. Iwai,[7] F. Jiménez-Espejo,[5] R. McKay,[8] S. Passchier,[9] J. Pross,[10] C. R. Riesselman,[11] U. Röhl,[12] F. Sangiorgi,[3] K. Welsh,[13] A. Klaus,[14] A. Fehr,[15] J. A. P. Bendle,[16] R. Dunbar,[17] J. Gonzàlez,[5] T. Hayden,[18] K. Katsuki,[19] M. P. Olney,[20] S. F. Pekar,[21] P. K. Shrivastava,[22] T. van de Flierdt,[23] T. Williams,[24] and M. Yamane[25]

Received 2 March 2012; revised 22 May 2012; accepted 23 May 2012; published 28 June 2012.

[1] The Integrated Ocean Drilling Program Expedition 318 to the Wilkes Land margin of Antarctica recovered a sedimentary succession ranging in age from lower Eocene to the Holocene. Excellent stratigraphic control is key to understanding the timing of paleoceanographic events through critical climate intervals. Drill sites recovered the lower and middle Eocene, nearly the entire Oligocene, the Miocene from about 17 Ma, the entire Pliocene and much of the Pleistocene. The paleomagnetic properties are generally suitable for magnetostratigraphic interpretation, with well-behaved demagnetization diagrams, uniform distribution of declinations, and a clear separation into two inclination modes. Although the sequences were discontinuously recovered with many gaps due to coring, and there are hiatuses from sedimentary and tectonic processes, the magnetostratigraphic patterns are in general readily interpretable. Our interpretations are integrated with the diatom, radiolarian, calcareous nannofossils and dinoflagellate cyst (dinocyst) biostratigraphy. The magnetostratigraphy significantly improves the resolution of the chronostratigraphy, particularly in intervals with poor biostratigraphic control. However, Southern Ocean records with reliable magnetostratigraphies are notably scarce, and the data reported here provide an opportunity for improved calibration of the

[1]Scripps Institution of Oceanography, University of California, San Diego, La Jolla, California, USA.
[2]Department of Geology, University of Tromsø, Tromsø, Norway.
[3]Marine Palynology, Department of Earth Sciences, Utrecht University, Utrecht, Netherlands.
[4]School of Ocean and Earth Science, University of Southampton, Southampton, UK.
[5]Instituto Andaluz de Ciencias de la Tierra, CSIC–Universidad de Granada, Armilla, Spain.
[6]Departamento de Geologia, Facultad de Ciencias, Universidad de Salamanca, Salamanca, Spain.
[7]Department of Natural Environmental Science, Kochi University, Kochi, Japan.
[8]Antarctic Research Centre, Victoria University of Wellington, Wellington, New Zealand.
[9]Earth and Environmental Studies, Montclair State University, Montclair, New Jersey, USA.
[10]Institute of Geosciences, University of Frankfurt, Frankfurt, Germany.
[11]Eastern Geology and Paleoclimate Science Center, U.S. Geological Survey, Reston, Virginia, USA.
[12]MARUM–Center for Marine Environmental Sciences, University of Bremen, Bremen, Germany.
[13]School of Earth Sciences, University of Queensland, Brisbane, Queensland, Australia.
[14]United States Implementing Organization, Integrated Ocean Drilling Program, Texas A&M University, College Station, Texas, USA.
[15]Institute for Applied Geophysics and Geothermal Energy, RWTH Aachen University, Aachen, Germany.
[16]Geographical and Earth Sciences, University of Glasgow, Glasgow, UK.
[17]Department of Geological and Environmental Sciences, Stanford University, Stanford, California, USA.
[18]Department of Geology, Western Michigan University, Kalamazoo, Michigan, USA.
[19]Quaternary Geological Research Department, Geological Research Division, Korea Institute of Geoscience and Mineral Resources, Daejeon, South Korea.
[20]Department of Geology, University of South Florida, Tampa, Florida, USA.
[21]School of Earth and Environmental Sciences, Queens College, Flushing, New York, USA.
[22]Antarctica Division, Geological Survey of India, Faridabad, India.
[23]Department of Earth Science and Engineering, Imperial College London, London, UK.
[24]Borehole Research Group, Lamont-Doherty Earth Observatory, Columbia University, Palisades, New York, USA.
[25]Earth and Planetary Science, University of Tokyo, Tokyo, Japan.

Corresponding author: L. Tauxe, Scripps Institution of Oceanography, University of California, San Diego, 9500 Gilman Dr., La Jolla, CA 92093-0220, USA. (ltauxe@ucsd.edu)

©2012. American Geophysical Union. All Rights Reserved.
0883-8305/12/2012PA002308

biostratigraphic records. In particular, we provide a rare magnetostratigraphic calibration for dinocyst biostratigraphy in the Paleogene and a substantially improved diatom calibration for the Pliocene. This paper presents the stratigraphic framework for future paleoceanographic proxy records which are being developed for the Wilkes Land margin cores. It further provides tight constraints on the duration of regional hiatuses inferred from seismic surveys of the region.

Citation: Tauxe, L., et al. (2012), Chronostratigraphic framework for the IODP Expedition 318 cores from the Wilkes Land Margin: Constraints for paleoceanographic reconstruction, *Paleoceanography*, *27*, PA2214, doi:10.1029/2012PA002308.

1. Introduction

[2] The initiation and development of glaciation on Antarctica had a profound effect on the Earth's climate and ocean circulation. Understanding of Antarctic climate evolution has far-reaching implications for Cenozoic climatic models. Expedition 318 of the Integrated Ocean Drilling Program (IODP) was designed to recover sedimentary archives documenting the entire history of climate on the Wilkes Land Margin from the Eocene greenhouse world up to the Holocene, including the onset of continental-scale glaciation at ~34 Ma. To obtain a sedimentary archive of Antarctic climate, Expedition 318 [*Escutia et al.*, 2011] drilled seven sites, three of which (U1356, U1359, and U1361, see Figure 1) are the focus of the present paper. *Escutia et al.* [2011] documented preliminary results from the expedition, including the identification of major regional hiatuses and biostratigraphic data. Here we present a state-of-the-art stratigraphic framework for the Wilkes Land drill cores. The chronostratigraphic constraints provided herein will serve as the basis for a robust timescale in which to interpret proxy-based paleo-records. These are aimed at improving our understanding of the dynamics and sensitivity of the Antarctic ice sheet, its development through time, and feedbacks on global climate system. The chronostratigraphy presented here is derived from updated results from both shipboard measurements as well as extensive shore-based investigations. Biostratigraphic data are revised and refined from those presented by *Escutia et al.* [2011] including new dinocyst and calcareous nannofossil data for the Paleogene, the Oligocene-Miocene transition within Hole U1356A, and improvements to the diatom stratigraphy for the Pliocene at Sites U1359 and U1361.

2. Methods

2.1. Continuous Measurement of Archive Halves

[3] Cores were split on board and the archive halves measured at 5 cm intervals using the shipboard 2G Enterprises cryogenic magnetometer. We measured the natural remanent magnetization (NRM) and the remanence after demagnetization in the in-line alternating field demagnetizer. Some archives were stepwise demagnetized to 5, 10, 15, 20 and 25 mT, but most were treated to a single demagnetization step of 15 (U1359D) or 20 mT (all remaining cores).

[4] Measurements of archives span the entire recovered section, including intervals disturbed by both sedimentary and drilling processes. In order to obtain the most reliable record possible, we inspected each core section using digitally enhanced photographs. Portions with contorted bedding, and microfaulting were removed, while minor core biscuiting was not. The Wilkes Land margin was at high latitude throughout the deposition of the recovered sequence (>60°S), so rotations about the vertical axis result in offsets in declination but the steepness of the directions allows discrimination of polarity based solely on the inclination. Other types of core disturbance (for example from the drilling process or from slumping) were also edited out. As discussed below, data from anisotropy of magnetic susceptibility were used to detect such drilling disturbances (see section 3.3). For more details on a site by site basis, please refer to *Escutia et al.* [2011].

2.2. Discrete Samples

[5] Discrete samples were taken typically one per 1.5 m core section. The naming convention used here is: the expedition number (here 318), the hole (e.g., U1356A), the core (e.g., 13 H, where 'H' stands for hydraulic piston core, 'X' for extended core barrel, and 'R' for rotary coring), the section number (1–7) and the top of the sampling interval in centimeters below the section top. In paleomagnetism, the term 'specimen' is generally used for objects that get measured, but there is no physical difference between the discrete samples and specimens in this study, so we will use the term 'sample' in this paper. A subset of the samples were subjected to stepwise alternating field (AF) demagnetization in fields of 5, 10, 15, 20, 30, 40 and (when strong enough) 50 and 60 mT on the ship. These were measured on the cryogenic magnetometer using a three step measurement protocol described in detail in the paleomagnetic methods section of *Escutia et al.* [2011]. In brief, each specimen axis was demagnetized and measured on each magnetometer axis. This protocol efficiently provides a robust estimate of the magnetization and also eliminates artifacts of anhysteretic remanence acquisition (ARM) during demagnetization. The rest of the samples taken during the cruise were demagnetized to either 15 mT or 20 mT. Shipboard samples from U1356A were used for other purposes and were unavailable for further paleomagnetic analysis, while all those from U1359 and U1361 were shipped to Scripps Institution of Oceanography (SIO). These and all samples taken after the cruise were stepwise demagnetized up to 80 mT in the paleomagnetic laboratory at SIO using a double demagnetization protocol [*Tauxe et al.*, 2010, chap. 9].

[6] In addition to AF demagnetization, the anisotropy of magnetic susceptibility (AMS) and bulk susceptibility were measured on all discrete samples either on the shipboard or shore-based Kappabridge KLY4S magnetic susceptibility instruments. Data were acquired with either the Sufar program supplied with the instrument or with the Labview program of

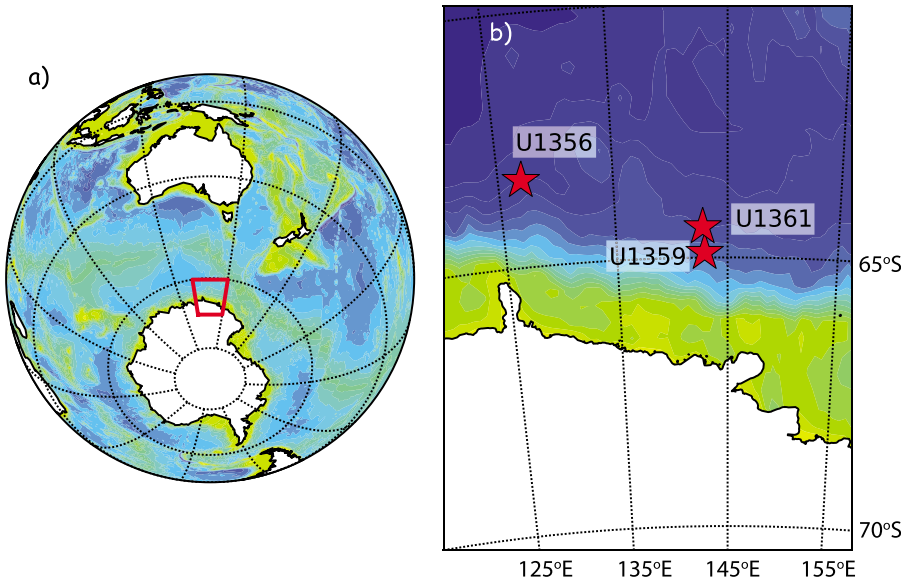

Figure 1. (a and b) Map of IODP Expedition 318 sites studied in this paper. Site U1356: 63.3102°S, 135.5994°E, 4003 meters below rig floor (mbrf). Site U1359: 64.5424°S, 143.5768°E, 3020 mbrf. Site U1361: 64.2457°S, 143.5320°E, 3466 mbrf.

Gee et al. [2008]. Multiple measurements on samples were averaged using Hext statistics [*Tauxe et al.*, 2010].

3. Results

[7] All paleomagnetic and rock magnetic data presented here have been contributed to the MagIC database (http://earthref.org/MAGIC/m000629dt20120607193954). Data can be reanalyzed and plotted using the PmagPy software package available at http://magician.ucsd.edu/Software/PmagPy. All of the plots and data analysis described below were done using this open source code.

3.1. Demagnetization Behavior

[8] Representative behavior of the Wilkes Land Margin sediments are shown in Figures 2 and 3. By far, the majority of samples that were fully demagnetized in the SIO laboratory behaved in a similar fashion to those shown in Figure 2. These exhibit univectorial decay to the origin after removal of a pervasive steeply down overprint, usually after demagnetization to 10 or 15 mT.

[9] We calculated a best-fit line (BFL) using principal component analysis [*Kirschvink*, 1980] and directions were deemed acceptable when based on a minimum of six consecutive demagnetization steps with a maximum angle of deviation (MAD) of less than or equal to 10°.

[10] Some samples did not display a smooth demagnetization to the origin (Figure 3). These were interpreted by calculating average directions from at least four consecutive measurements with Fisher statistics [*Fisher*, 1953]. The directions of these are lower quality than those based on principle component analysis, but were deemed sufficient for reliable polarity determination if the α_{95} was less than or equal to 15°.

3.2. Data Quality

[11] Cryogenic magnetometers are sufficiently sensitive that the remanence of most samples can be measured. It is always necessary to establish that the remanence vectors record a geomagnetic signal and not a diagenetic, tectonic, coring disturbance-related signal or drill string overprint of no value for magnetostratigraphy. For a successful magnetostratigraphic study, we require that the characteristic remanence be confidently isolated as demonstrated by stepwise demagnetization. The directions must belong to two distinct directional modes (normal and reverse). For high latitude sites, histograms of the inclinations from the edited archive half measurements and the principal component analysis on discrete samples should show two distinct "humps". Moreover, for core material that is not azimuthally oriented, the declinations from core to core, or from distinct pieces within the cores, should be uniformly distributed with no preferred orientation.

[12] The histograms of inclinations from the Wilkes Land sites (Figures 4a–4c) show a clear separation into two modes as expected from these high latitude sites. Because the Wilkes Land margin was at high southerly latitudes throughout its history, we interpret the negative inclinations (up) as being normally magnetized.

[13] The histograms of the declinations are not as straightforward as for the inclinations. The data from the archive half measurements seem to be sinusoidally distributed with a minimum likelihood near the antipode to the double line (X direction in sample coordinates). Quantile-quantile plots of declinations allow a powerful statistical test for uniformity based on a Kolmogorov-Smirnov test statistic M_u [*Fisher et al.*, 1987] and *Tauxe et al.* [2010, chap. 11]. Because of the strong downward directed overprint (presumably from the drill string), evident in the demagnetization data (Figures 2 and 3), it is possible that a bias caused by overprinting or core splitting behaves differently for the two directional modes. Therefore, we plot the declinations of those vectors associated with upward-directed inclinations (red dots) and downward directed inclinations (blue dots) separately in Figure 5 for the three different sites. The data

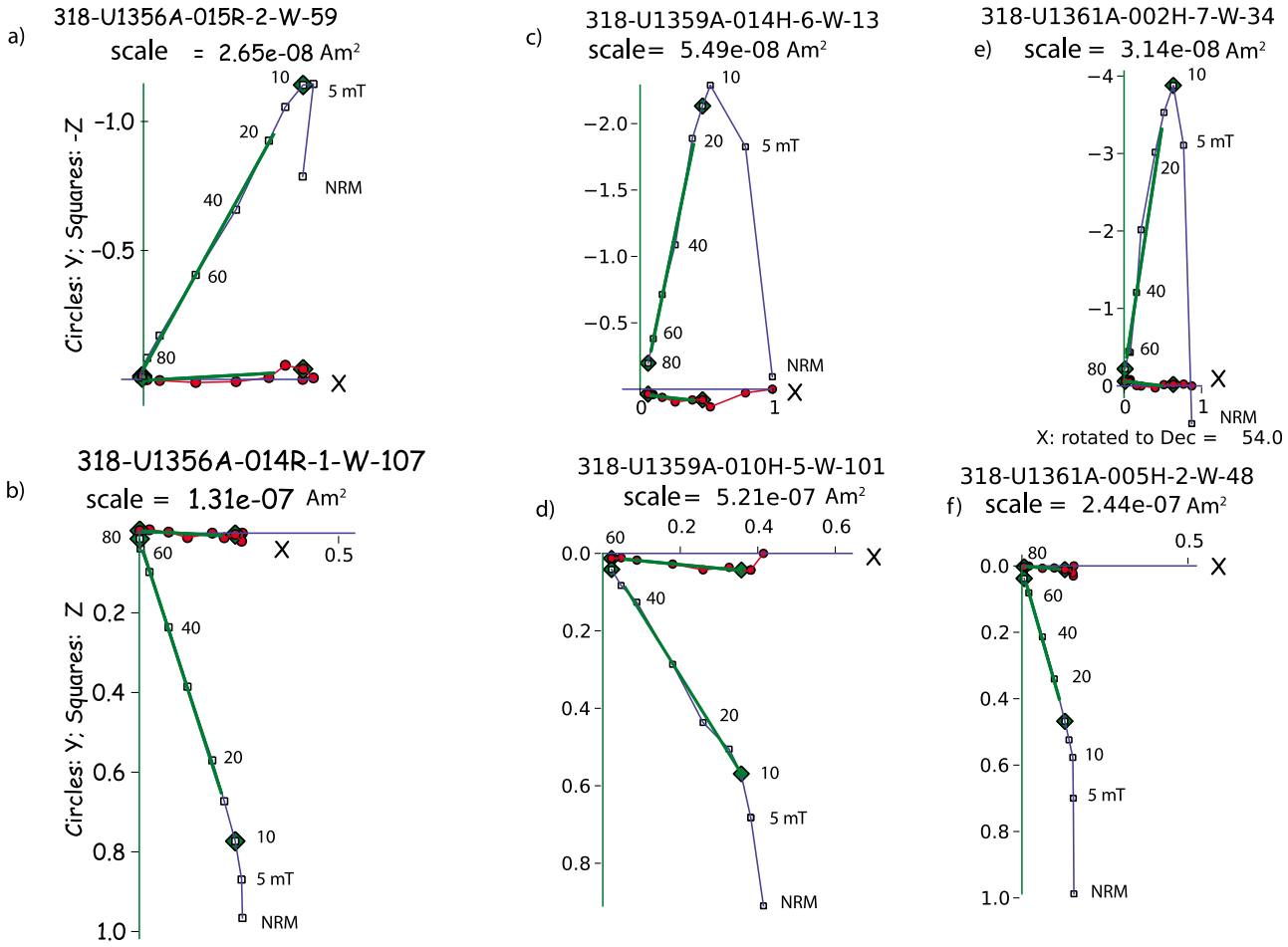

Figure 2. Examples of the most common behavior of discrete samples during stepwise alternating field demagnetization plotted as vector end-point diagrams. Solid (open) symbols are in the horizontal (vertical) planes. Sample naming convention: EXPEDITION-HOLE-CORE-SECTION-HALF-INTERVAL where W is working half and interval is in centimeters below the top of the section. (a, c, e) Up directions are normal and (b, d, f) down directions are reverse. The steep downward directed component removed by 10 or 15 mT is the "drilling remanence". The green lines connecting two diamonds are the best-fit lines.

from the archive halves are the left-hand panels and the M_u statistic shows that all but the declinations associated with downward directed inclinations for U1356 and those associated with upward inclinations at Site U1359 are unlikely to have been drawn from a uniform distribution. They are indeed biased at the 95% level of confidence. However, the distribution of declinations from the best-fit lines of discrete samples from sites U1356 and U1359 appear much more uniform. Only those associated with upward directed best-fit lines from U1361 fail at the 95% level of confidence (but pass at the 99% level of confidence).

[14] Previous researchers have attributed observed biases in declinations to radial overprints caused by distortion of beds during coring [*Acton et al.*, 2002]. Others have pointed to off-centered measurement of split halves in the magnetometer [*Parker*, 2000; *Parker and Gee*, 2002]. In the case of the Wilkes Land sites, the present geomagnetic field direction is nearly straight up. Coring disturbance generally bends layers downward along the side of the core liner, resulting in an average magnetization with a bias away from the X direction and not toward it as observed in Figure 4. *Parker* [2000] explains the bias toward the X direction by measuring cores with center of mass below the magnetometer axis and predicts a bias along the Z and X directions. From his analysis, it seems quite likely that the bias is an artifact of measuring archive halves off-center in the magnetometer. This bias should not be present in the discrete samples and in fact, is not.

[15] Because the best-fit lines derived from stepwise demagnetization data appear to conform to the requirements of a reliable magnetostratigraphy and both the archive halves and best-fit lines appear to have two modes of inclination, we will interpret the remanence vectors as reflecting the geomagnetic field at the time of deposition (or nearly so). The most reliable intervals are those with agreement between the more sparsely distributed discrete sample data and the data from the archive halves. In intervals where the two do not agree, the greatest weight should be placed on the best-fit lines, then on the Fisher means, and last on the archive halves alone.

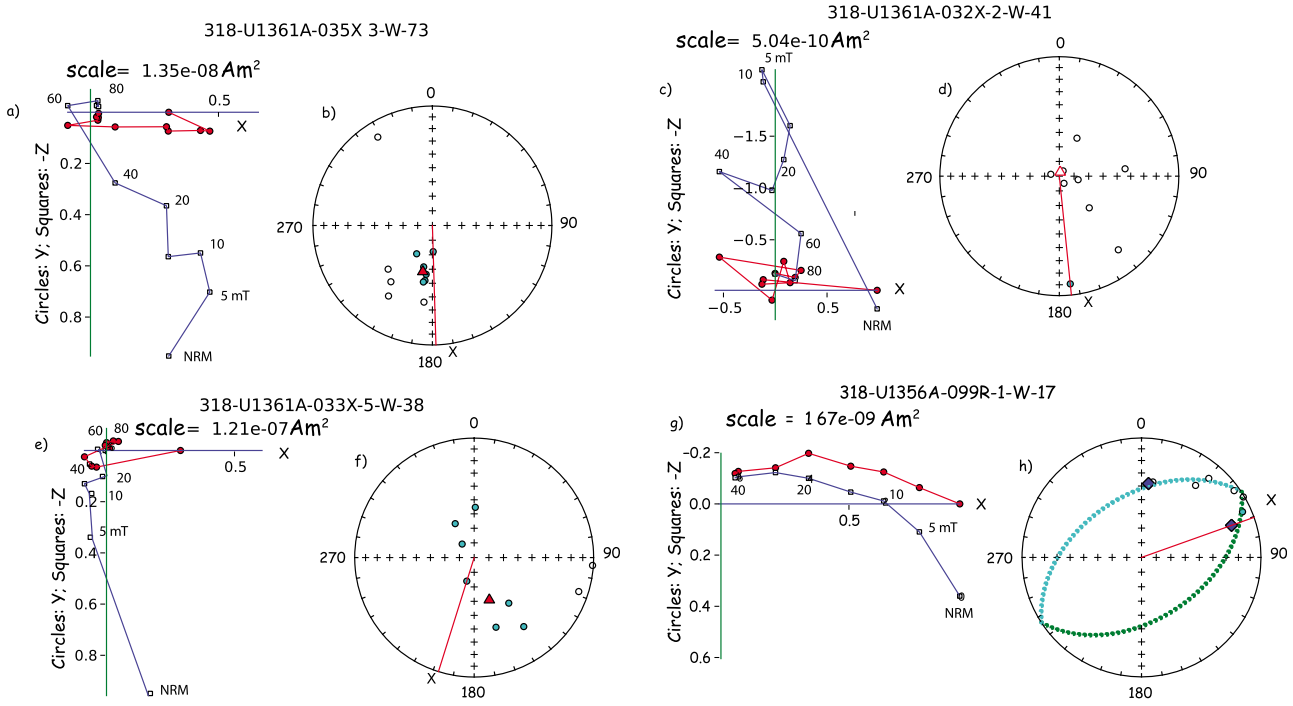

Figure 3. (a, c, e, g) Same as Figure 2 but for data treated by averaging unit vectors (Fisher means) or blanket AF demagnetization. (b, d, f, h) Equal area projections of directions during demagnetization. Solid (open) symbols are lower (upper) hemisphere projections. Red triangles are Fisher means. Dashed line in Figure 3h is great circle with green line on lower hemisphere. Figures 3g and 3h are best interpreted as a great circle trend with no stable direction. Such data were not used for magnetostratigraphic interpretations.

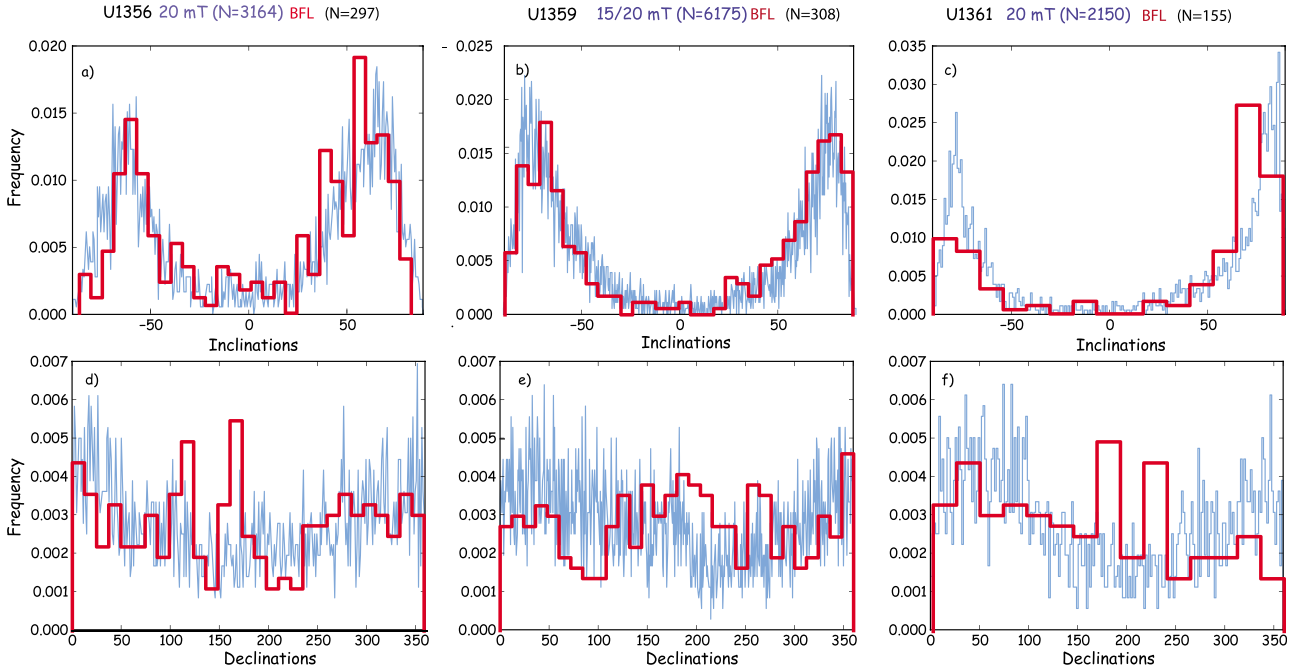

Figure 4. Histograms of (a–c) inclinations and (d–e) declinations from Wilkes Land cores. Archive halves after demagnetization to 15 or 20 mT are plotted as light blue lines. Acceptable best-fit lines from stepwise demagnetization data ($N_{meas} \geq 6$; MAD $\leq 10°$) are plotted as heavy red lines. Figures 4a and 4d are for Site U1356, Figures 4b and 4e are for Site U1359, and Figures 4c and 4f are for U1361.

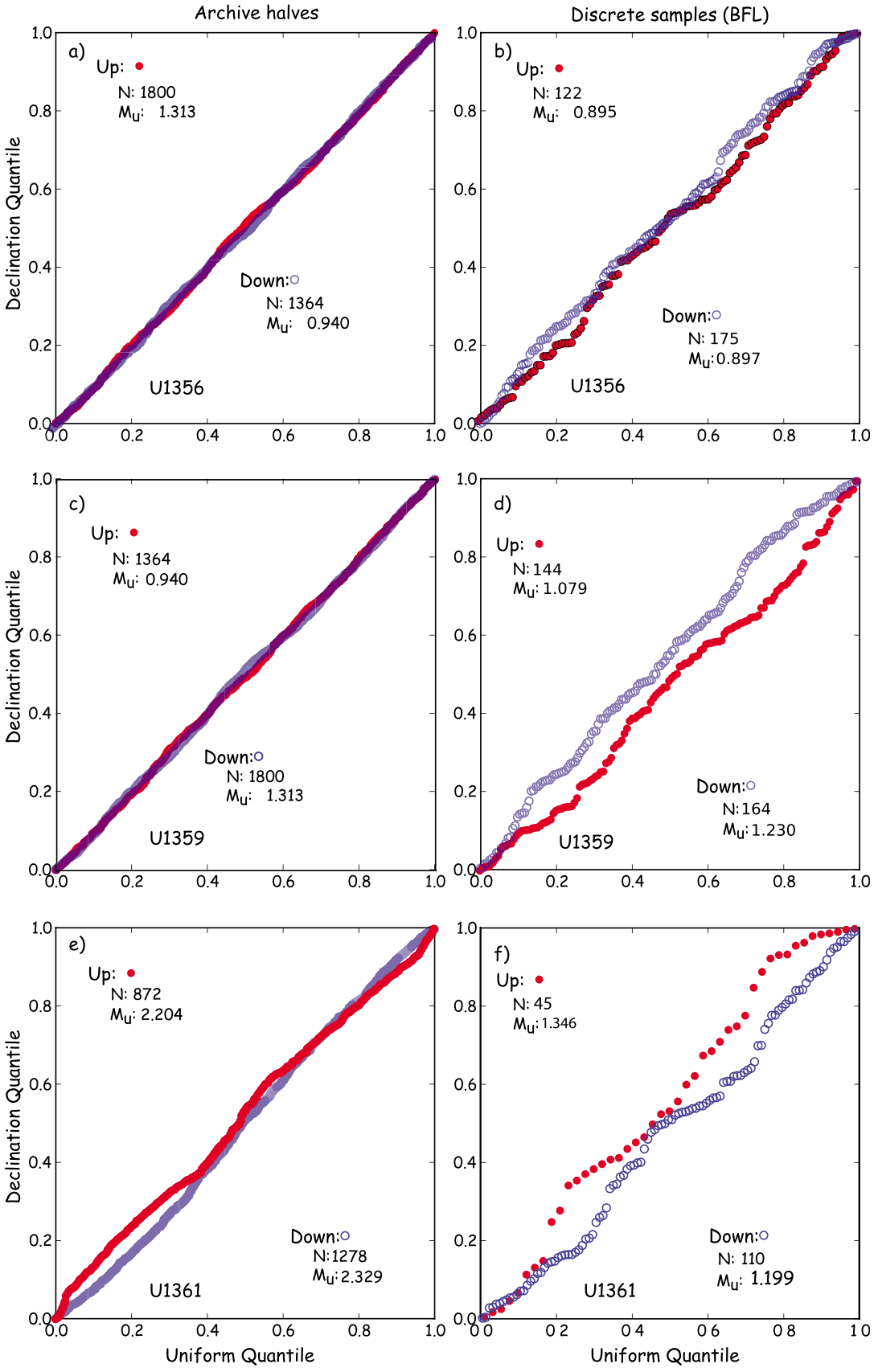

Figure 5. Quantile-Quantile plots of declinations from (a, c, e) archive halves and (b, d, f) discrete sample best-fit lines against a uniform distribution. A uniform distribution can be excluded at the 95% level of certainty if the value of $M_u \geq 1.207$ or at the 99% level of certainty if $M_u \geq 1.347$ (see text).

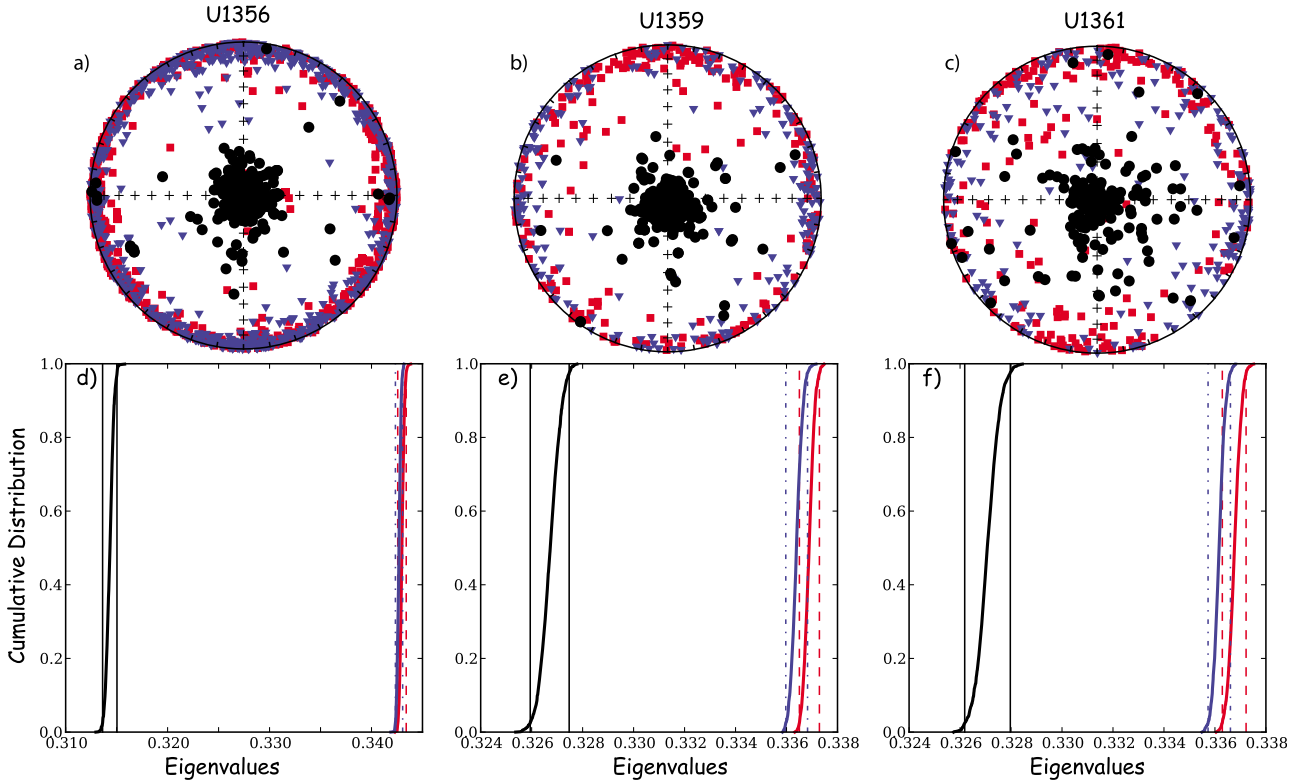

Figure 6. Anisotropy of magnetic susceptibility for Sites U1356, U1359 and U1361. (a–c) Equal area projections of the eigenvectors associated with maximum, intermediate and minimum susceptibility ($\mathbf{V_1}$, $\mathbf{V_2}$, $\mathbf{V_3}$), respectively. Black dots: $\mathbf{V_3}$, blue triangles: $\mathbf{V_2}$; red squares: $\mathbf{V_1}$. (d–f) Cumulative distributions of eigenvalues of bootstrapped pseudosamples of AMS data. Maximum (τ_1), intermediate (τ_2) and minimum (τ_3) shown as red, blue and black lines. The 95% confidence bounds are vertical lines. The means of τ_1 and τ_2 are indistinguishable, hence the fabric is on average oblate.

3.3. Anisotropy of Magnetic Susceptibility

[16] Results for the anisotropy of magnetic susceptibility (AMS) are shown for the three sites in Figure 6. In general, the data for all three sites have vertical axes of $\mathbf{V_3}$, the axis of minimum susceptibility (black circles in Figures 6a, 6b, and 6d). The $\mathbf{V_2}$ and $\mathbf{V_1}$ axes, or intermediate (red triangles) and maximum (blue squares), respectively, are distributed near the horizontal plane. In order to assess the shapes of the AMS ellipsoids, we use the bootstrap approach of *Constable and Tauxe* [1990] described in *Tauxe et al.* [2010, chap. 11]. Bootstrapped eigenvalues are plotted as cumulative distributions in Figures 6d–6f for the three sites. The bounds containing 95% of the bootstrapped values are shown as vertical lines. In all three cases, the maximum (τ_1) and intermediate (τ_2) eigenvalues (red and blue lines respectively) are statistically indistinguishable, while the minimum eigenvalues τ_3 (black lines) are quite distinct. The AMS fabric is therefore oblate [*Tauxe et al.*, 2010, chap. 13]. The characteristics of quasi-vertical axes of minimum susceptibility and oblate fabrics are typical of undisturbed sedimentary fabrics.

[17] While most of the samples are indeed oblate with near vertical $\mathbf{V_3}$ axes, some of the fabrics are either triaxial or isotropic and/or have $\mathbf{V_3}$ axes that are quite displaced from the vertical (see especially the data from Site U1361 in Figure 6c). Such data were taken as a sign of disturbed fabrics and those intervals were eliminated from the magnetostratigraphic study.

[18] One measure of the degree of anisotropy is the ratio of τ_1/τ_3, usually termed P [*Tauxe et al.*, 2010, chap. 13]. The AMS data from the deepest hole, U1356A, is the most anisotropic, with values of $P \sim 1.09$ on average compared to that from U1359 and U1361 of $\sim$1.03 on average. This reflects the fact that the primary control on sedimentary fabric development is compaction [*Schwehr et al.*, 2006]. Changes in anisotropy degree can result from compaction disequilibria resulting from changes in lithology, for example alternating between diatom-rich and diatom-poor layers, or from hiatuses. The former will be discussed elsewhere, while the latter will be explored in section 4.1.2.

3.4. Magnetostratigraphy

[19] Inclinations from Sites U1356, U1359 and U1361, are plotted versus depth in Figures 7, 8, 9, and 10. Data from continuous measurements are shown as translucent dots while best-fit lines and Fisher means from discrete samples are shown as red triangles and cyan diamonds respectively. As anticipated from the histograms, the discrete sample data generally agree well with the continuous measurements and nearly all of the polarity intervals detected in the archive measurements are confirmed by stepwise demagnetization of discrete samples.

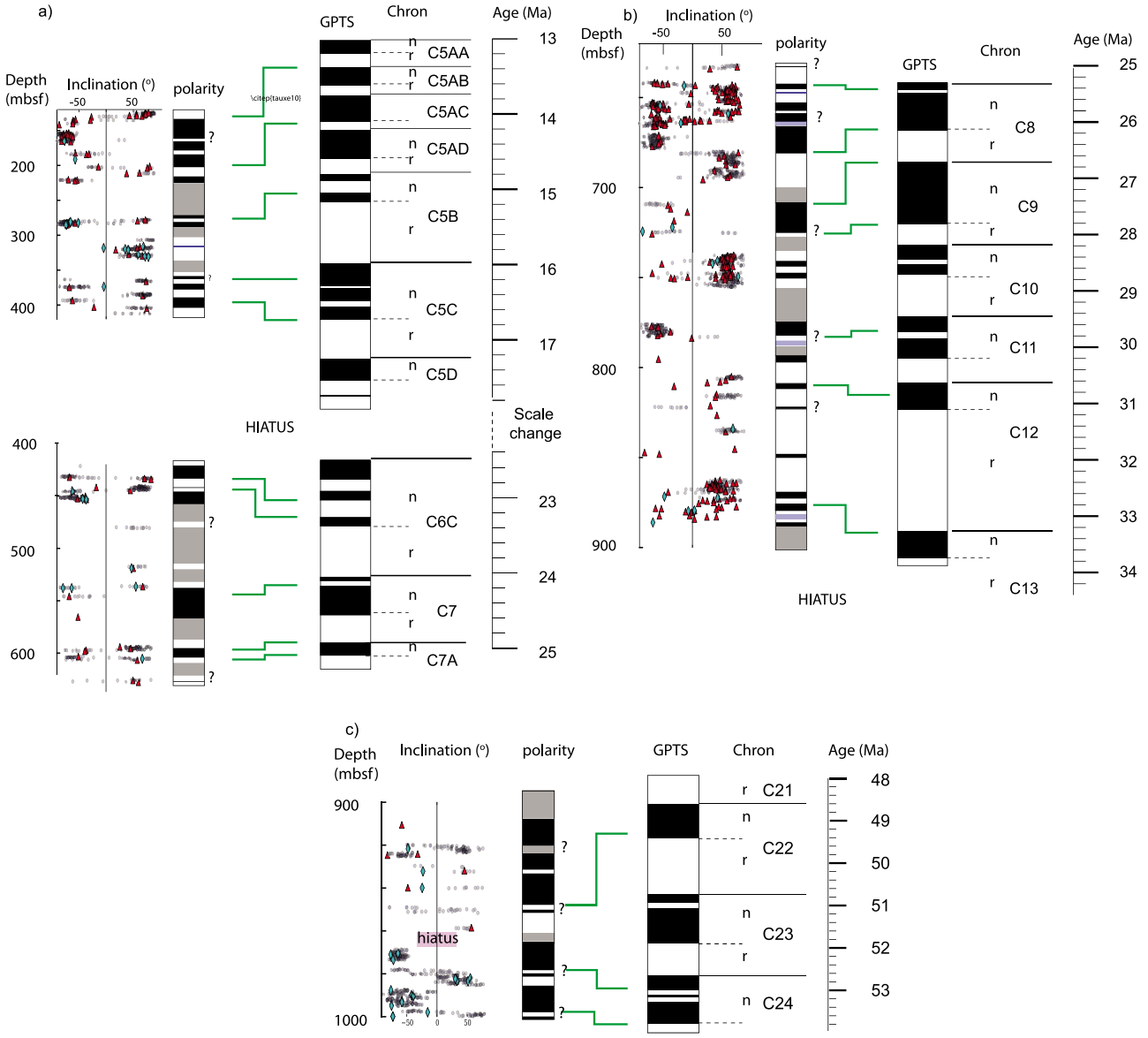

Figure 7. Magnetostratigraphic data from U1356A. Small blue dots are data from the archive halves demagnetized to 20 mT (edited according to details in the text). Red triangles are acceptable best-fit lines. Cyan diamonds are acceptable Fisher means. Black intervals in the polarity log are normal, white are reverse, blue are ambiguous polarity, and grey are intervals with no data. Question marks denote polarity intervals based solely on shipboard measurements. In Geomagnetic Polarity Timescale (GPTS), black intervals are normal polarity and white are reverse. Blue intervals are zones with near horizontal inclinations that are of indeterminate polarity. Chrons are calibrated as in the Geological Timescale of *Gradstein et al.* [2004]. Green tie lines are as listed in Table S1. (a) Top 625 mbsf, (b) 625–900 mbsf, and (c) 900–1000 mbsf.

[20] Positive inclinations are interpreted as reverse while negative inclinations are normal but intervals with data within 10° of the horizontal are difficult to interpret as to polarity. Intervals with ambiguous polarity are shaded blue in the polarity logs and intervals based solely on archive half data are indicated with a question mark. Long intervals with no data are shown as grey bars.

[21] The polarity logs are correlated to the geomagnetic polarity time (GPTS) shown to the right. For consistency with other investigations of the Wilkes Land scientific party, we use the calibration of *Gradstein et al.* [2004] for the GPTS. Identification of particular chron boundaries is notoriously difficult in discontinuously sampled records, especially in continental margins, where hiatuses are expected. Our strategy for the Wilkes Land margin magnetostratigraphic data was to find the correlation to the GPTS with the fewest gaps and the most constant sedimentation rates possible. Hiatuses or changes in sediment accumulation rate are only inserted as demanded by the magnetostratigraphic or biostratigraphic data. For the latter, we rely on the

[1]Auxiliary materials are available in the HTML. doi:10.1029/2012PA002308.

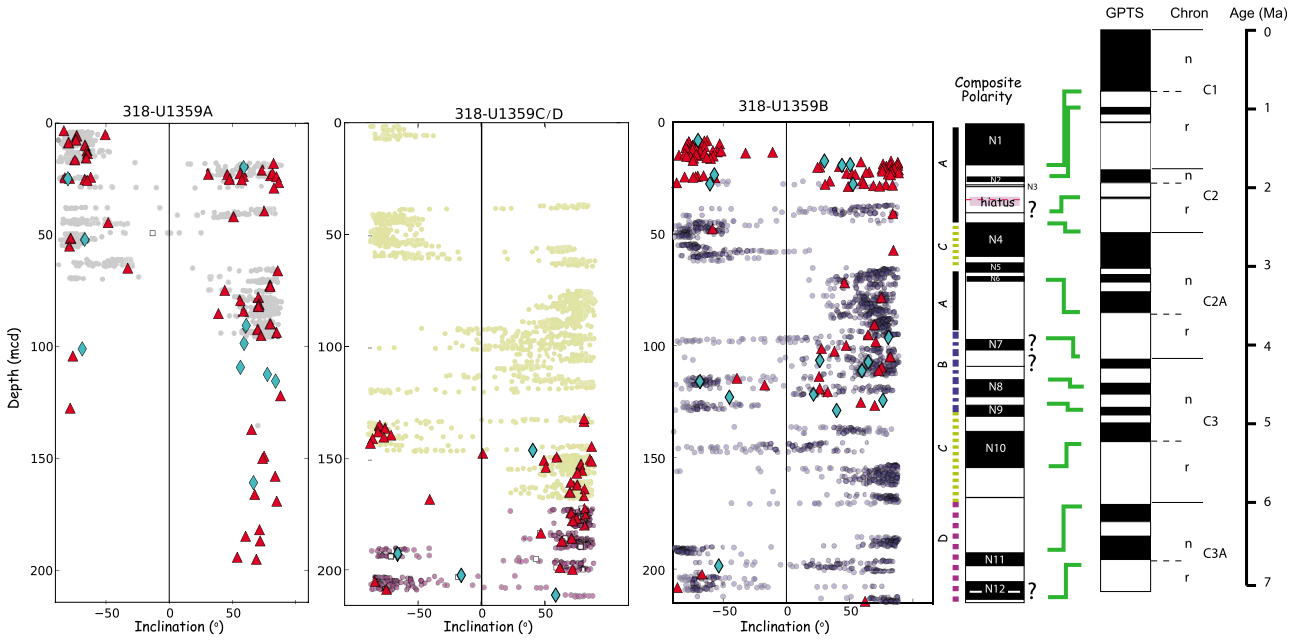

Figure 8. Top 215 meters of Site U1359, plotted on composite depth scale (mcd). Symbols same as in Figure 7 except archive half data are color-coded by hole with U1359A: grey, U1359B: blue U1359C: yellow and U1359D: magenta. Colored dashed and solid lines marked A,B,C,D adjacent to the Composite Polarity indicate the hole for which the magnetic data is presented. Tie points as listed in Tables S2–S4.

biostratigraphic constraints as published by *Escutia et al.* [2011] as well as updated tie points determined post-cruise (Tables S1-S6 in the auxiliary material).[1] Our preferred correlations of the magnetostratigraphy to the GPTS are shown as heavy green lines.

4. Discussion

4.1. U1356

4.1.1. Correlation to the GPTS

[22] Hole U1356A was rotary cored for its entire length. The top 100 meters were badly disturbed by the coring process and we do not consider the data from this interval here. We were able to fit the polarity intervals for the rest of the hole with the GPTS by dividing the record into four intervals with nearly uniform sediment accumulation rates. The top interval, spanning from ~100 to ~400 meters below seafloor (mbsf) ranges in age from about 13 to 17 Ma, based on diatom and (sparse) radiolarian events (Table S1 and Figure 11). It correlates reasonably well to Chrons C5AAr through C5Cr as shown in Figure 7a. While recovery was discontinuous, all of the polarity intervals are represented.

[23] Below 400 mbsf, it was impossible to correlate the magnetostratigraphic pattern to the GPTS continuing down from C5Cr without extreme variations in sediment accumulation rate (Table S1 for Chron boundary identifications). Furthermore, examination of the calcareous nannofossils revealed the last occurrence (LO) of *Reticulofenestra bisecta* (Table S1 and Figure 11) at 431.48 mbsf. This event is one of the ways of recognizing the base of the Miocene [*Steininger et al.*, 1997] although it cannot be recognized at the Global Boundary Stratotype Section and Point itself due to reworking. However, its highest occurrence in Hole 522A occurs in core 3, section 1 between 20 and 60 cm or 59.2–59.6 mbsf [*Percival*, 1984], or just below the onset of C6C.2n [*Shackleton et al.*, 2000] (note that in *Percival* [1984], *Reticulofenestra bisecta* was referred to as *Dictyococcites bisectus*). Based on this last occurrence (LO), we can identify the onset of C6C.2n at 432.77 mbsf in U1356A. Above this, there must be a hiatus spanning the interval from just above C5D to just above C6Cn.2n, or approximately seven million years. Based on the magnetostratigraphic interpretation shown in Figure 7 and Table S1, we constrain the position of hiatus to be between about 402 and 432 mbsf. It is therefore at least 28 meters above a major lithologic change from diamictites in the lithologic logs (boundary between lithological Units III and IV at 459.4 mbsf from [*Escutia et al.*, 2011] and shown in Figure 11).

[24] The interval from 430 mbsf to 883 mbsf has sparse biostratigraphic control (Table S1 and Figure 11), with only a few radiolarian events and one foraminiferal event. Nonetheless, it is possible correlate the magnetostratigraphic record to the GPTS from Chrons C6Cn.2n to C13n by assuming two linear sedimentation rates. The change in sediment accumulation rate from about 89 m/m.y. to about 28 m/m.y. is at about 653 mbsf, within lithologic Unit V (593.8–694.4 mbsf [*Escutia et al.*, 2011]).

[25] The LOs of calcareous nannofossils *Reticulofenestra umbilicus* and *Isthmolithus recurvus* 883.34 ± 2.6 mbsf [*Escutia et al.*, 2011] (Table S1) and the first occurrence (FO) of the dinocyst *Malvinia escutiana* at 894.68 mbsf (Table S1) provide some constraints for the identification of the poorly resolved normal interval between 878 and 883 mbsf in Figure 7b as C13n. The highest common occurrence of *R. umbilicus* at 106 mbsf and the highest occurrence of *I. recurvus* at 109 mbsf in Site 748B [*Fioroni et al.*, 2012] places these events in the top and bottom of

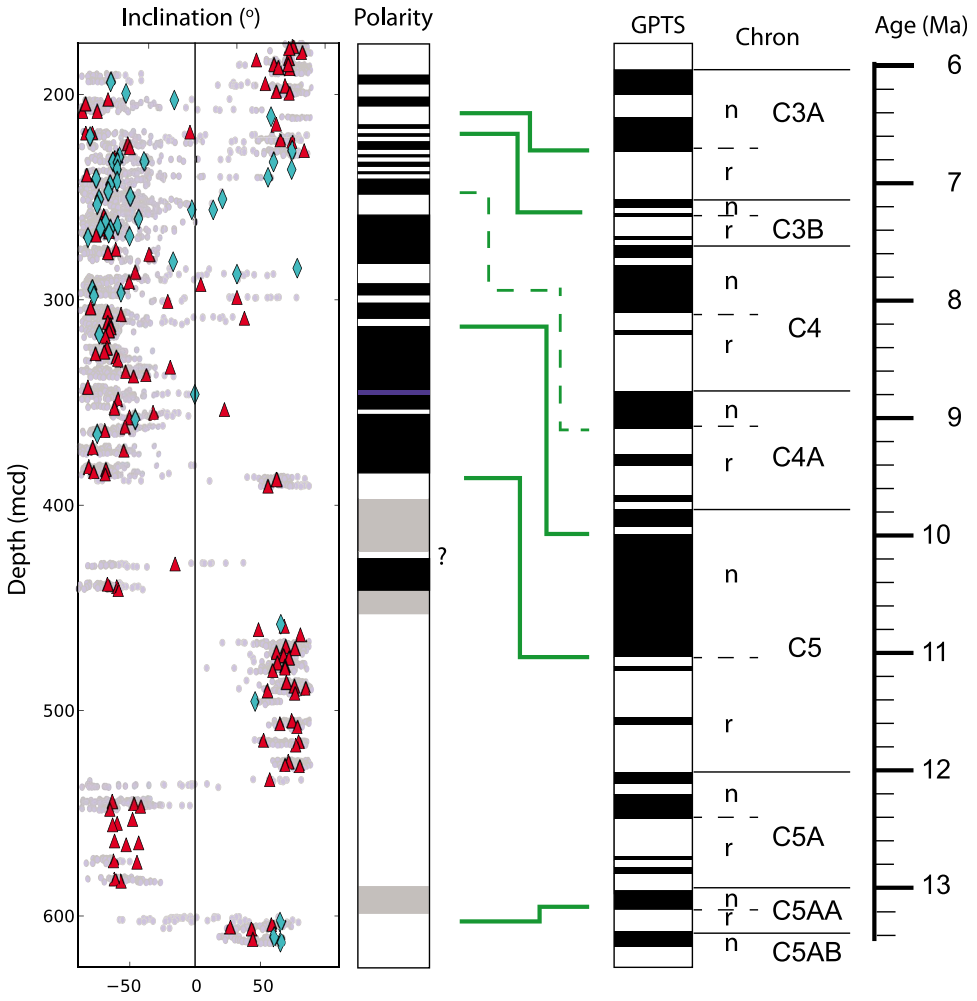

Figure 9. Bottom part of site U1359, plotted on meters composite depth (mcd). Symbols same as in Figure 7. Dashed green line is a best-guess correlation. Tie points as listed in Table S5.

Chron C12r, respectively, based on the magnetostratigraphy of *Roberts et al.* [2003]. The FO of *M. escutiana* was tied to the Oi-1 isotopic event by *Houben et al.* [2011], while Oi-1 event is itself tightly associated with Chron C13n at Site 522 [*Miller et al.*, 1991] using the magnetostratigraphy of *Tauxe et al.* [1983]. It was also found at the base of Chron C13n at Site 689 by *Bohaty et al.* [2012] using the magnetostratigraphy of *Florindo and Roberts* [2005]. Thus the interval between 878 and 883 mbsf in U1356A is likely to be Chron C13n.

[26] Contorted bedding interrupted our ability to correlate to the GPTS in the interval between about 883 and 895 mbsf. Lithologic Unit IX (879.7–895.5 mbsf in *Escutia et al.* [2011]), is thought to result from submarine slides and slumps. However, in the sample at 894.71 mbsf, just below the FO of *Malvinia escutiana* (894.68 mbsf), we find the last *in situ* occurrence of *Membranophoridium perforatum*, thought to be middle Eocene in age (Table S1). This, combined with the absence of *Enneadocysta multicornuta* and *E. dictyostila*, suggests a hiatus spanning at least the latter 13 million years of the Eocene within Core 95R between these two samples. The dinocyst assemblages at the bottom of the hole contain *Impagidinium cassiculum* and *Samlandia delicata* which are loosely tied to an early Eocene calcareous nannofossil assemblage in New Zealand [*Crouch and Brinkhuis*, 2005]. Hence, the age of the oldest strata recovered is early Eocene. We will describe the Eocene bio-magneto-stratigraphy below in more detail.

[27] The inclination log for 900–1000 mbsf of U1356A (Figure 7c) could be correlated to the GPTS from Chrons C23n to C24r with no major change in sediment accumulation rate required. The abundant palynomorphs should in principle allow us to correlate directly to the GPTS using the prevailing age model for dinocyst stratigraphy in the Southern Ocean [*Bijl et al.*, 2010; *Bijl*, 2011]. However, this relies on the interpretation of the magnetostratigraphy of ODP Site 1172 which is based not on the inclination data from Site 1172 (as is the usual practice), but on a 20 point running average of the 'Z' (vertical) component of the magnetization vectors after demagnetization to 20 mT [*Fuller and Touchard*, 2004]. The rationale for the unusual approach to 1172 is depicted Figure 12. While the inclination data show no clear distinction between normal (negative) and reverse (positive) modes with a single negative mode, there are two 'humps' in the vertical component ('Z') data. This component is obtained by the formula $M \sin(I)$ where M is the remanent intensity and I is the inclination. Hence, the data shown in black in the inset are

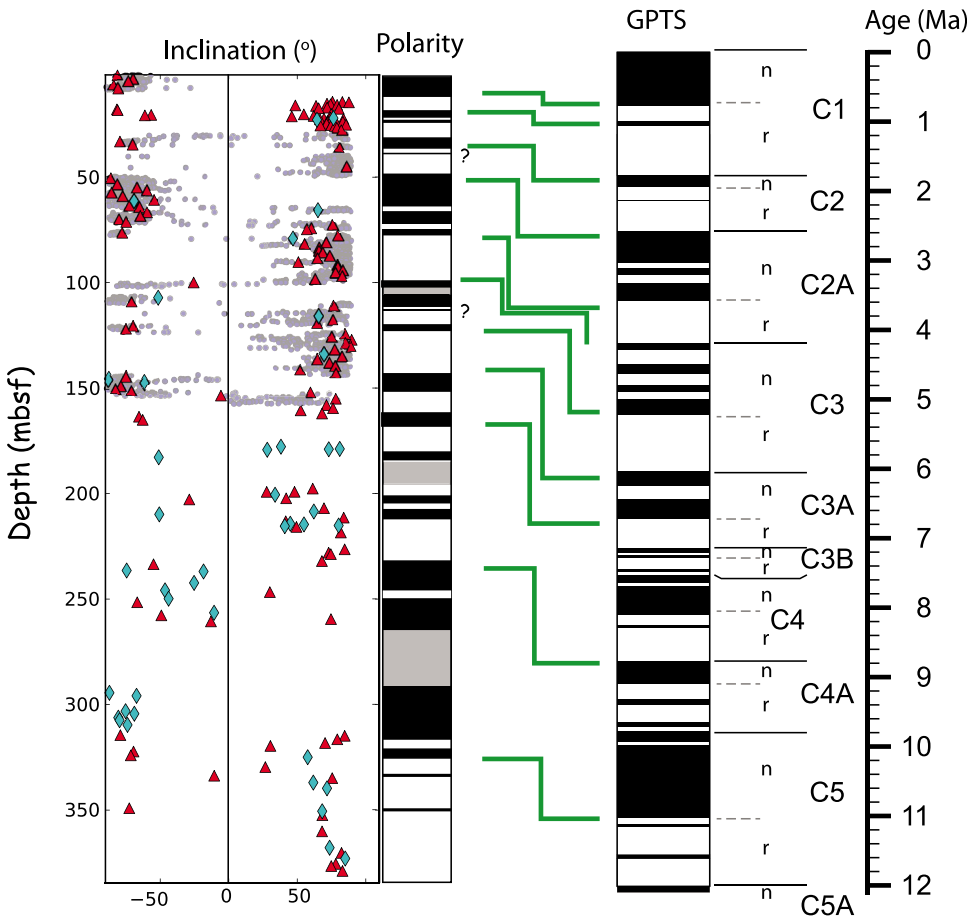

Figure 10. Same as Figure 7 but for Hole U1361A. Paleomagnetic tie points as listed in Table S6.

dependent on the intensity of the magnetization vector, while the inclination itself is not. If we plot instead the vertical component of the unit vectors (assuming $M = 1$, see red curve in the inset), we see only one distinct 'hump' and a long tail, similar to the inclination data. The alternating positive and negative intervals obtained from the vertical full vector component, after subtraction of the mean, served as the basis for the magnetostratigraphic interpretations. This apparent polarity zonation is an artifact of relying entirely on the strength of the remanence vector (black versus red curves in the inset to Figure 12).

[28] The interpretation of using NRM intensity as a proxy for polarity stratigraphy is based on the idea that there is a strong overprint in the vertical (up) direction in these sediments [*Fuller and Touchard*, 2004] (as opposed to the downward directed drill string remanence seen in the Expedition 318 sediments). An upward directed overprint nearly antiparallel with a downward reverse direction leads to an overall weaker remanence for reversely magnetized NRMs relative to the normal NRMs which have the same upward directed overprint added to them. Therefore, if this overprint were the only contribution to intensity variations, the two intensity humps could be reasonably attributed to polarity, if the overprint were insufficiently removed. However, there are also large swings in intensity caused by variations in lithology. Intervals with more magnetic material in them (silts versus carbonates) also have stronger intensities. Lithologic controls on intensity cannot be easily separated from unremoved overprints and the large swings in NRM intensity cannot be reliably tied to polarity. Indeed, no demagnetization diagrams have been published from this record that we know of, and the case for unremoved overprints as the sole control on NRM intensity has not been made. It is therefore unwise to use intensity fluctuations as the basis for magnetostratigraphic correlation to the GPTS. Fortunately, sections in New Zealand have tied dinocyst events to nanoplankton stratigraphy [*Hollis et al.*, 2009], which enables indirect correlation of the dinocyst stratigraphy to the GPTS.

[29] In Figure 13a we show an expanded version of the magnetostratigraphic data for the lowermost section of Hole U1356A from Figure 7c along with a polarity log based largely on interpretation of demagnetization of discrete samples. We also show key dinocyst events [*Bijl*, 2011; *Escutia et al.*, 2011] (Table S1). Various dinocyst events common to U1356A as well as the FO and LO of the calcareous nannofossil *Discoaster kuepperi* from Site 1172 are shown in Figure 13b. These are from *Bijl* [2011] and *Wei et al.* [2004] respectively. The *Charlesdowniae* dinocyst events are also seen in the Ashley Mudstone sequence in New Zealand (Figure 13c) in which they can be placed relative to the LO of *D. kuepperi* as well as the LO of calcareous nannofossils *Discoaster lodoensis* and *Tribrachiatus orthostylus* [*Hollis et al.*, 2009]. The latter was directly tied

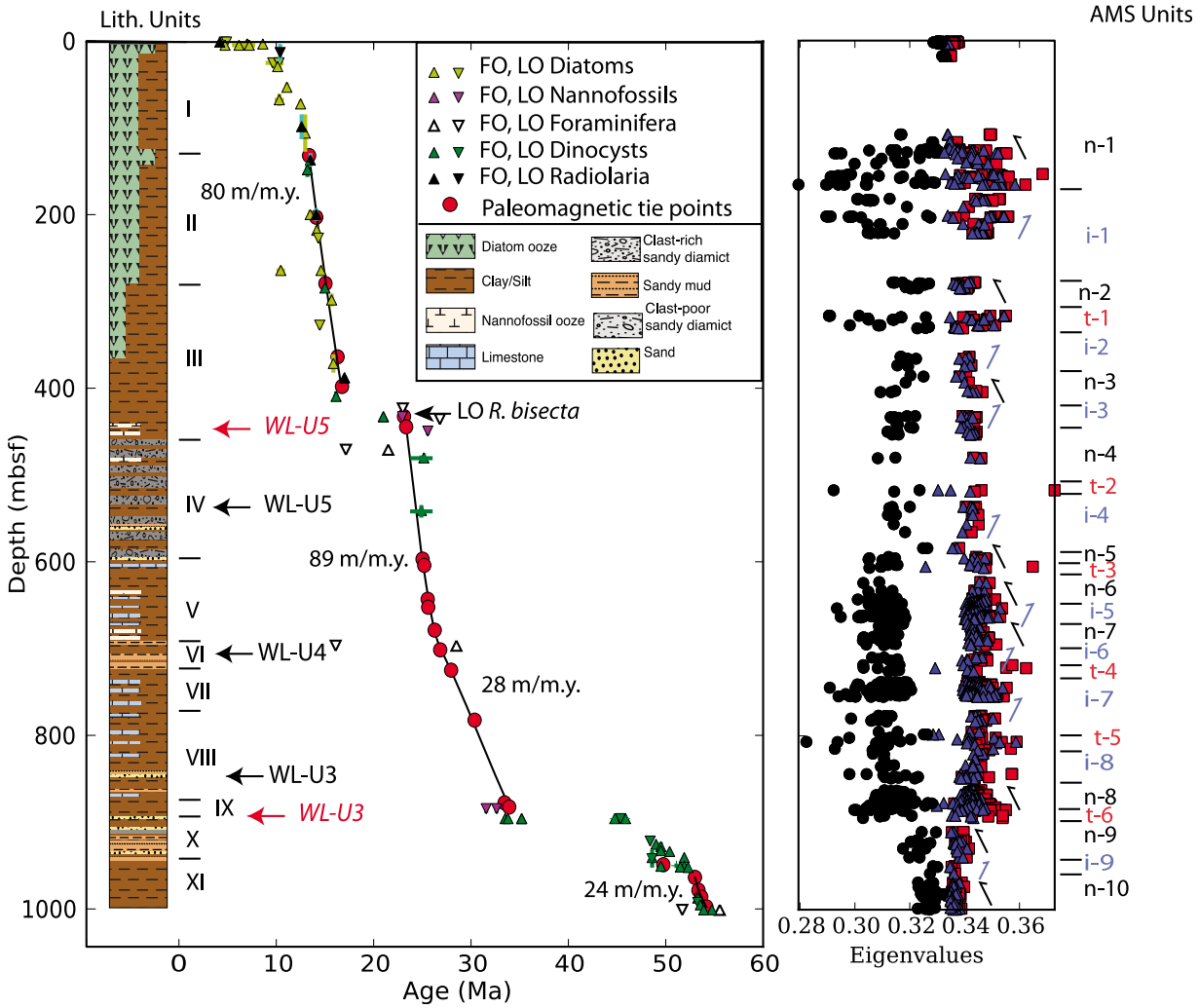

Figure 11. Age-depth plot for U1356A. Lithostratigraphic summary from *Escutia et al.* [2011] and biostratigraphic constraints from *Escutia et al.* [2011] and Table S1. Last occurrence (LO) and first occurrence (FO) include last common and last abundant occurrences (LCO and LAO, respectively). Same for FCO and FAO in FO. Paleomagnetic tie points are as in Figure 7 and Table S1. Uncertainties in age and position of biostratigraphic datums indicated by horizontal and vertical bars respectively. Anisotropy of magnetic susceptibility (AMS) data plotted as eigenvalues: squares are τ_1, triangles are τ_2 and circles are τ_3. Normal and inverse trends in AMS are indicated with upward trending arrows to the left and right (blue) respectively. AMS intervals with normal (n-1–n-10), inverse (i-1–i9) oblate fabrics and triaxial (t-1–t-6) fabrics are marked to the right. Seismic horizons in black (red) are the original (revised) depths in *Escutia et al*. [2011].

to the GPTS in the Possagno Section in Italy [*Agnini et al.*, 2006] and lies virtually coincident with the top of Chron C23n. The LO of *D. lodoensis* occurs in C21r [*Agnini et al.*, 2006] as shown in Figure 13d.

[30] Because the dinocyst events occur above the LO of *T. orthostylus* (which marks the onset of C22r), their appearance in the normal zone spanning the Core 98R and the top of 99R in Hole U1356A (921–932 mbsf, N1) suggests that this normal zone is most likely C22n. The pollen and spores in 101R and 100R suggest a profound change in paleoenvironment on the Antarctic margin consistent with a shift from a paratropical rain forest to a temperate rain forest ecosystem [*Pross et al.*, 2012]. There is also a change in the lithostratigraphy (Unit XI/X boundary) between Cores 98R and 99R at 948.8 msf, and the lowest position of sand layers with erosional bases in 100R (at about 940 mbsf, see Figure 11). Pulling all these lines of evidence together suggests that N2 is part of C22n, which has a small reverse interval within it, not included in the GPTS and the hiatus occurs between 100R and 101R, removing all or most of C23n. We were unable to obtain usable discrete samples from core 101R and the scattered data from the archive half with polarity interpretations marked with a question mark may or may not represent the onset of C23n.

[31] *Payros et al.* [2011] investigated both magnetostratigraphy and calcareous nannofossil biostratigraphy in the Otskakar section of northern Spain. They located the CP12a/CP12b boundary within Chron C21r and provide a

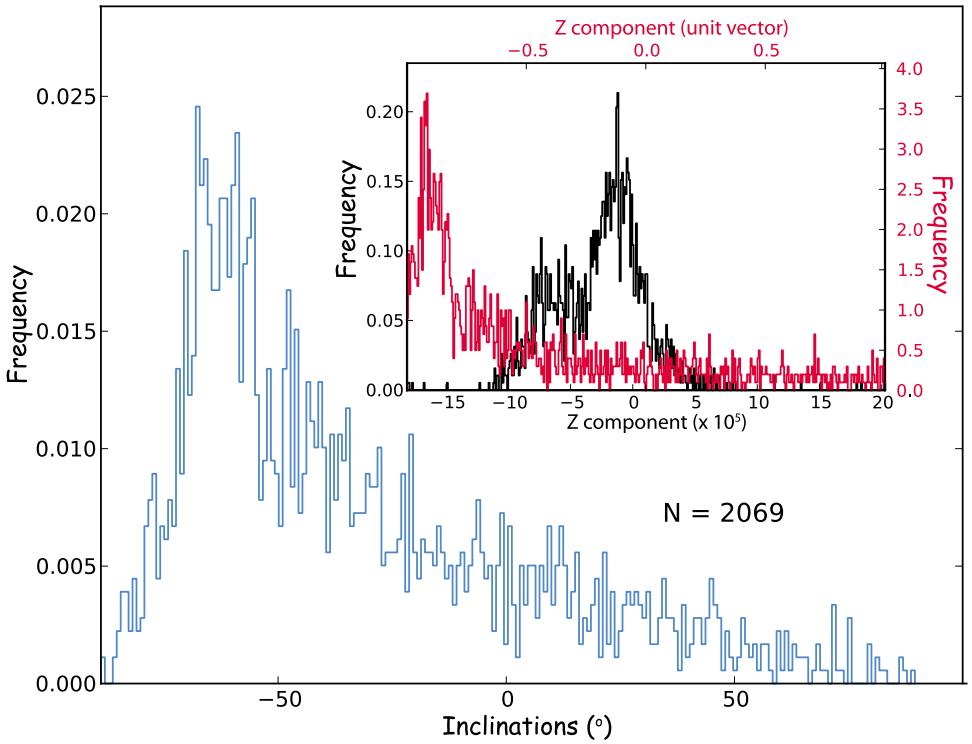

Figure 12. Histogram of inclination data after demagnetization to 20 mT from ODP Site 1172D between 500 and 625 mbsf obtained from the JANUS database at http://iodp.tamu.edu/janusweb/paleomag/cryomag.shtml. Inset is of the vertical component of the same data with black using the full vector and red using unit vectors. The magnetostratigraphic interpretations for Site 1172 relied on the data shown in black, hence only on the magnetization strength and not its direction.

new calibration of the middle and early Eocene boundary at about 47.76 Ma. This suggests that the entire section below 920 mbsf is early Eocene in age.

4.1.2. Anisotropy of Magnetic Susceptibility

[32] Results of our AMS experiments are plotted to the right of Figure 11. We plot the eigenvalues (τ_1, τ_2, τ_3) as squares, triangles and circles respectively in the stratigraphic log. One of the main controls on the degree of anisotropy P, reflected by the spread between τ_1 and τ_3 in the figure, is the degree of compaction. Under normal sedimentary conditions, compaction would decrease monotonically up core, indicated by the leftward trending arrows to the right of the AMS log. Intervals with this normal trend are labeled n-1 through n-10 to the right.

[33] Inverse AMS trends reflect compaction disequilibria [*Schwehr et al.*, 2006] which can result from a variety of causes. For example, an impermeable layer that prevents dewatering results in a less compacted layer in the zone with excess water. A layer with abundant diatoms or sand will not compact as well as layers of silt or clay. Contrasts in compaction regimes can result from hiatuses as well. It is interesting to note that all of the abrupt changes in sediment accumulation rates, including major hiatuses discussed in the foregoing are marked by inverse AMS intervals. The hiatus above 432 mbsf is immediately underlain by inverse interval i-3. The change in sedimentation rate at 653 mbsf is within i-5. Finally, the hiatus inferred at 948.8 mbsf corresponds to i-9.

[34] Both the normal and inverse trends in AMS degree are associated with oblate fabrics. There are, however, a few horizons with markedly triaxial fabrics, labeled t-1–t-6. Triaxial fabrics point to disrupted sedimentary fabrics and five out of six of these are in intervals with claystone intraclasts (too small for the lithologic log). The major hiatus between the early Eocene and the Oligocene sediments at 895 mbsf marks an abrupt change in AMS fabrics between n-9 and t-6.

4.2. Site U1359

4.2.1. Correlation to the GPTS

[35] The upper 215 meters of Site U1359 was triple-cored with the advanced piston corer and extended core barrel (Holes U1359A, B, C). The lower part, extending down to below 600 mbsf, was rotary cored at Hole U1359D. A composite depth scheme was developed based on physical properties in *Escutia et al.* [2011], allowing the data to be plotted against meters composite depth (mcd) for this site. Paleomagnetic data for the top 215 meters are shown in Figure 8. The composite polarity log was constructed using the best record for each interval out of the four holes. The hole from which each segment is derived is indicated to the left of the composite polarity log. Normal polarity zones are numbered for convenience. An expanded version of the top 30 m of Holes U1359A and U1359B is also shown in Figure 15 and the paleomagnetic data from the lower portion of U1359D are shown in Figure 9.

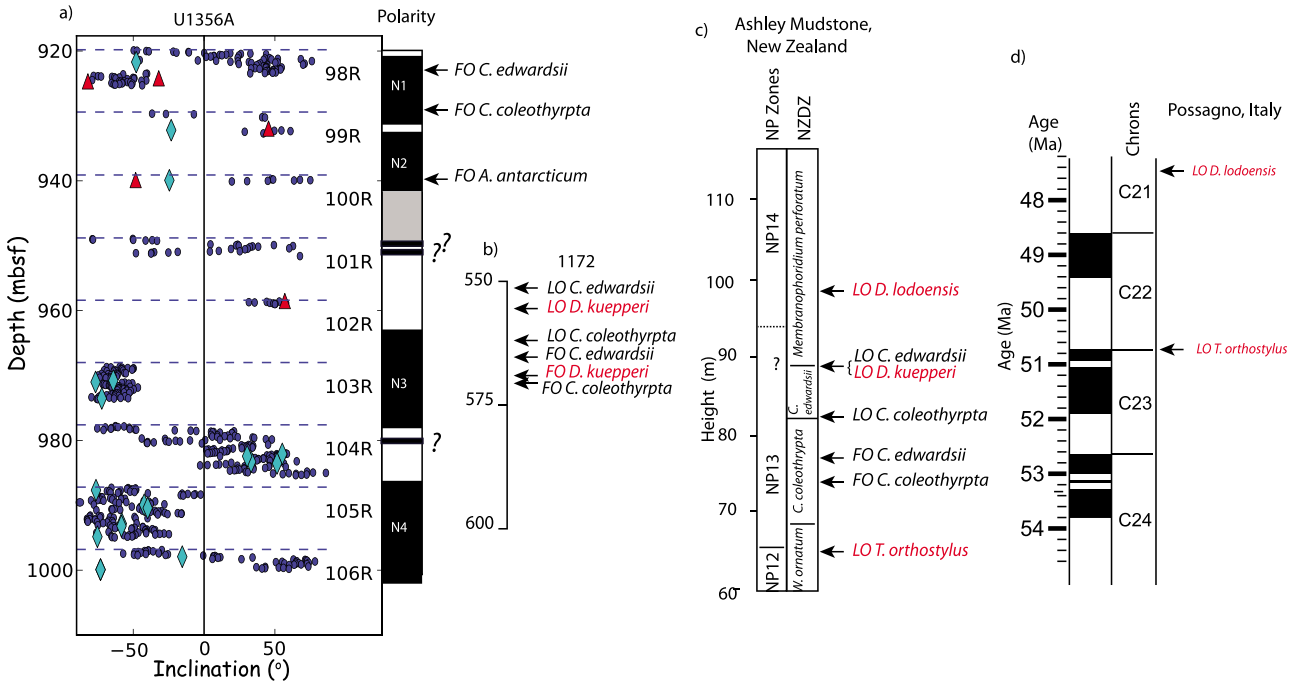

Figure 13. Calibration of dinocyst zonation. (a) U1356A magnetostratigraphic data from Figure 7. Dinocyst events from *Escutia et al.* [2011] and Table S1. (b) Dinoflagellate stratigraphy from ODP Site 1172 [*Bijl*, 2011]. The first and last occurrences (FO and LO) for *D. kuepperi* (red) are from *Wei et al.* [2004]. (c) Calcareous nannofossil (in red) and dinocyst occurrences in the Ashley Mudstone sequence, mid-Waipara River section. Modified from *Hollis et al.* [2009] supplementary material. (d) Last occurrence of *T. orthostylus* with respect to the geomagnetic polarity timescale of *Gradstein et al.* [2004] based on magnetobiostratigraphy in the Possagno Section in Italy [*Agnini et al.*, 2006].

[36] Biostratigraphic constraints for Site U1359 are based on radiolarian and diatom events, summarized by *Escutia et al.* [2011] (Tables S2–S5 and Figure 14). The available data support the correlation of N1 in Figures 8 and 15 to the Brunhes (Chron C1n). The Brunhes/Matuyama boundary (Chron C1n (o)) occurs at 17.87 and 17.28 mcd in Holes U1359A and U1359B respectively (Tables S2, S3, and Figure 15).

[37] The interval labeled N2 in Figures 8 and 15 is correlated to the Jaramillo (Chron C1r.1n) with the top of this boundary at 24.13 and 23.90 mcd in U1359A and U1359B respectively. The sedimentation rates in each of these cores are identical, i.e., ~24 m/m.y. to the top of the Jaramillo. Therefore, N3 in U1359A at 25.79 mcd is likely to be the Punaruu (1.092 Ma) [*Channell et al.*, 2008]. Compared to U1359A, N3 in U1359B occurs significantly lower at ~27 mcd and, assuming a constant sedimentation rate, is consistent with N3 being the Cobb Mountain (Chron C1r.2n). The expected composite depth for the location of the Punaruu in U1359B is extremely disturbed by drilling and was not sampled for magnetostratigraphy. Similarly, the expected depth for the Cobb Mountain in U1359A has an internal stratigraphy that is complicated by inclined bedding [*Escutia et al.*, 2011], and therefore this subchron could not be not replicated in the magnetostratigraphy for U1359A owing to a sampling gap (Figure 15).

[38] Returning to Figure 8, N4 in the composite polarity log occurs between 41.38 and 41.43 mcd, and could thus be the Olduvai (C2n). However, the reverse interval above it is "too short" necessitating a substantial decrease in the sediment accumulation rate or a hiatus between the Jaramillo/Punaruu and the Olduvai. The LOs of a number of diatom species however suggest that the Olduvai is missing entirely and that N4 is instead the top normal zone of the Gauss (C2An.1n). Assuming that this is the case, there is no trouble correlating zones N4 through N12 in Figure 8 to Chrons C2A through C3A. All of the subchrons in the GPTS are present and no significant changes in sediment accumulation rate are required to accommodate the correlation.

[39] The lower part of U1359D from about 215 mcd to below 600 mcd (Figure 9) is more difficult to tie to the GPTS. The location of the site on a channel levee [*Escutia et al.*, 2011] means high sediment accumulation rates accompanied by significant hiatuses. Nonetheless, the identification of Chron C5n.2n from about 308 to 386 mcd is reasonably secure and is consistent with the (sparse) radiolarian events in this interval (Figure 14). Similarly, the identification of C5AAn (o) at about 603 mcd is in fair agreement with constraints provided by radiolarian FO of *Desmospyris megarocephalis* and the diatom FOs of *Fragilariopsis claviceps* and *Denticulopsis praedimorpha s.l.* (Tables S2–S5). This interpretations implies an average sediment accumulation rate of over 100 m/m.y. The interval between Chrons C3Ar and C4Ar are difficult to correlate uniquely to the GPTS and the identification of Chron C4An is tentative.

[40] Despite good agreement between the magnetostratigraphy correlation and the biostratigraphic events in the

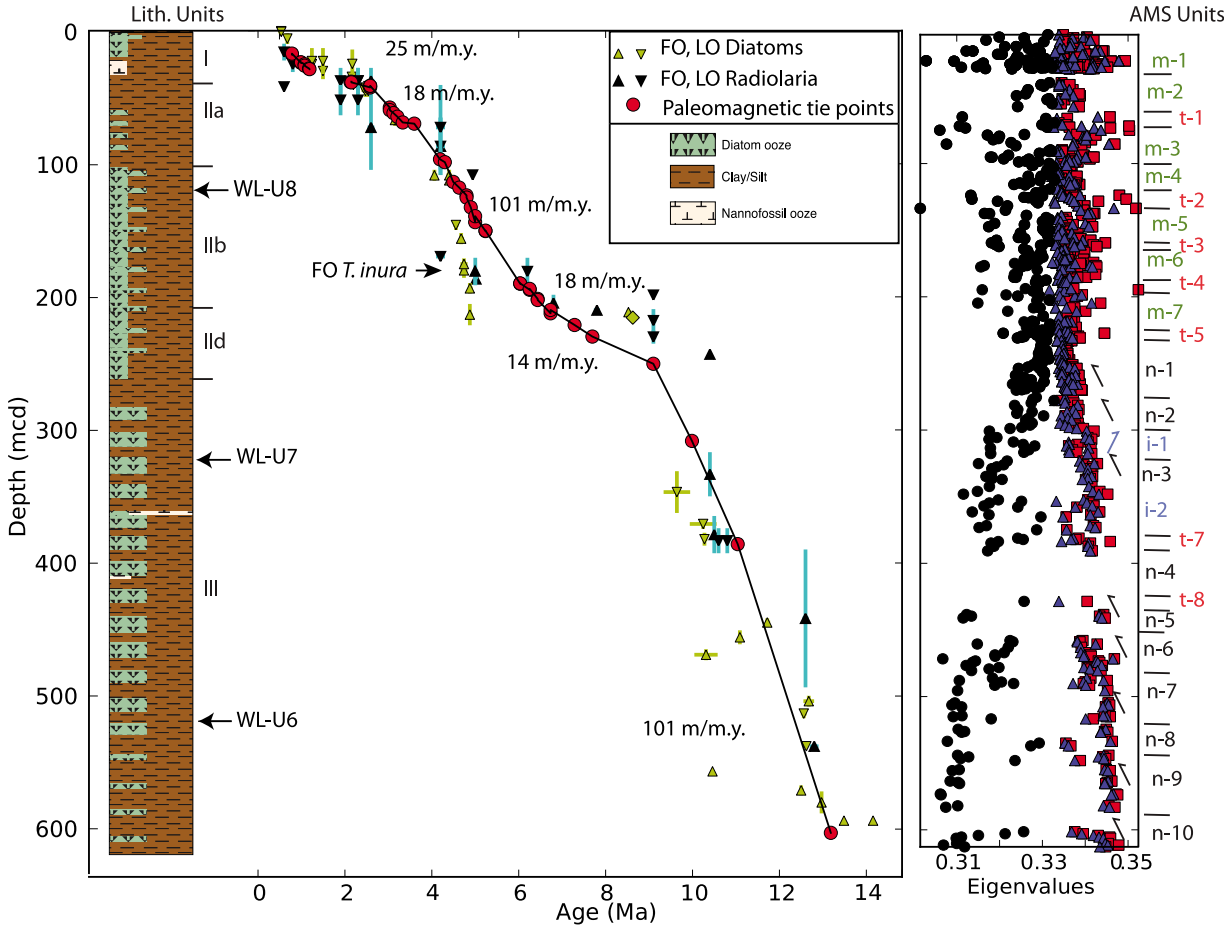

Figure 14. Same as Figure 11, but for U1359 composite in mcd. Paleomagnetic tie points are as in Figures 8 and 9 and listed in Tables S2–S5.

top and bottom of Site U1359, it is ironic that the part with the most convincing magnetostratigraphic correlation to the GPTS, polarity zones N4 to N12, has a relatively poor agreement with the ages inferred from the observed diatom events (see *Escutia et al.* [2011] and Tables S2–S5). This interval has long been troublesome [*Iwai et al.*, 2002]. While a detailed analysis of this problem is beyond the scope of this paper, we will examine one of the most discrepant diatom events, the FO of *Thalassiosira inura.* This event, at ~175 mcd or in the middle of C3r, would be ~5.9 Ma according to the age model for Site U1359. However, the diatom age model used by Expedition 318 [*Cody et al.*, 2008] dates the FO of *T. inura* at 4.74 ± 0.03 Ma (median age of the Average Range Model), a discrepancy of over a million years, while noting that the published dates range from 4.8 to 6.83 Ma. The datum of *Cody et al.* [2008] is a constrained optimization model age based on the FO of *T. inura* in multiple DSDP, ODP, and nearshore continental shelf sites, representing a range of Southern Ocean environments some of which have direct magnetostratigraphic calibration as summarized in their supplemental material. Most of the magnetostratigraphic interpretations from sites incorporated in the *Cody et al.* [2008] model are poor at best, with many inferred hiatuses or drastic changes in sediment accumulation rates. Some are in intervals that the authors themselves deemed 'unresolved' or were based on the NRM data only with no demagnetization and no clear distinction between the two polarities. However, a few do have well-resolved magnetostratigraphies. ODP Holes 745B and 690B (*Sakai and Keating* [1991] and *Spieß* [1990], respectively) place the datum within C3r (consistent the interpretation suggested here). These are located within the modern zone of winter sea ice as are Sites U1359 and U1361.

[41] In contrast, ODP Site 1091 [*Channell and Stoner*, 2002] is located at the northern margin of the modern polar frontal zone, and places the *T. inura* event in the Gauss (Chron C2A), or some three million years later. The diatom age model of *Cody et al.* [2008] assigned an age that is the mid point between these two calibration points. Based on the data presented here, it appears that the older age of *Sakai and Keating* [1991] is closer to the absolute FO of *T. inura* and is concordant with our interpretation. These observations also highlight the importance of considering latitudinal or environmental diachroneity in the evolution and extinction of biostratigraphically important species. We note that the magnetostratigraphic correlation of U1359A in the interval of Chron C3r appears to be more robust than any of the others cited for this interval and should therefore serve as a reference section for future Pliocene Southern Ocean biostratigraphy.

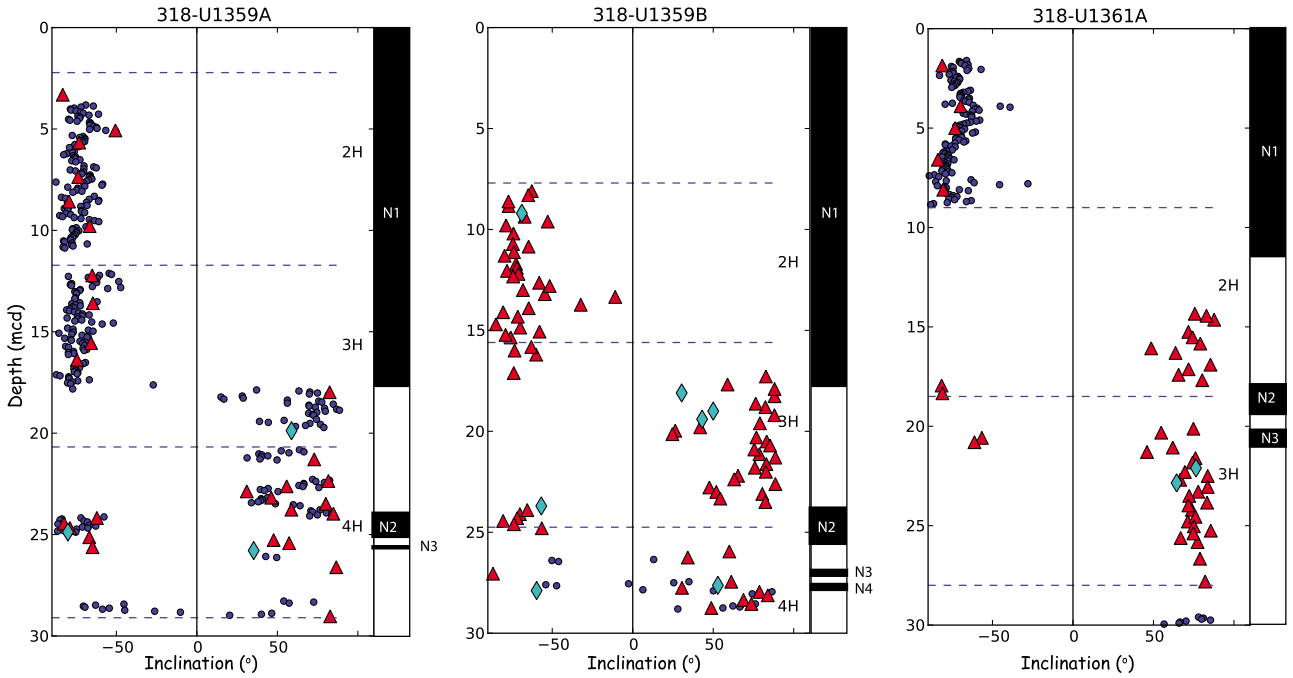

Figure 15. Expanded plot of top 30 meters in cores with Jaramillo (C1r.1n). Data for U1359 are from Figures 8 and those from U1361A are from Figure 10. N2 in all holes is likely to be the Jaramillo. N3 is found at a shallower depth in U1359A than in U1359B (in mcd). Depth scale of U1361 is in mbsf.

4.2.2. Anisotropy of Magnetic Susceptibility

[42] The AMS stratigraphy for Site U1359 is shown to the right of Figure 14. There are eight "triaxial" horizons, the top five of which occur at inferred changes in sediment accumulation rates based on the magnetostratigraphic correlation discussed in the previous section. Unlike at Site U1356, the AMS stratigraphy has only two intervals with inverse anisotropy trends (i-1, i-2). The interval i-2 appears to correspond with a horizon composed of nannofossil ooze. The lower half of the site, comprising lithologic Unit III is a sequence of superposed normal compaction packages, from n-2 to n-10. This interval has a relatively high anisotropy degree of ~1.12 on average. From n-2 to n-1, there is an overall reduction in anisotropy degree with $P \sim 1.02$ at the top of n-1. This unit is topped by triaxial unit t-5 and marks the base of the very low sediment accumulation rate interval approximately comprising lithologic Unit IId. Lithologic Units I, IIa and IIb are quite different in their AMS behavior from the lower part of the section in that, instead of packages characterized by normal compaction, the AMS behavior is quite mixed with alternating layers of high and low anisotropy degree. These correspond to diatom-poor and diatom-rich layers respectively, a behavior which will be discussed in more detail elsewhere. Here, we simply refer to these intervals as "mixed" and label them m-1 through m-7. The m-1/m-2 boundary corresponds to the hiatus associated approximately with the lithologic Unit I/IIa boundary.

4.3. Site U1361

4.3.1. Correlation to the GPTS

[43] The magnetostratigraphic data for U1361A are shown in Figure 10 and the biostratigraphic constraints in Figure 16. The bottom of the Brunhes (C1n (o)) is not well constrained owing to drilling disturbance between 8.10 and 14.34 mbsf. However, assuming a relatively constant sedimentation rate of ~18 m/m.y., constrained by the top of the core and the top of the Jaramillo (Chron C1r.1n) at 17.95 mbsf, the Brunhes/Matuyama boundary would be expected to occur near the bottom of the disturbed interval, i.e., near ~14 mbsf. As at Site U1359, there is a short double normal zone between 17.68 and 21.07 mbsf (N2 and N3 in Figure 15), which is likely to be the Jaramillo and Cobb Mtn pair, assuming a relatively linear sedimentation rate with minimal hiatuses. This assumption is supported by the lithostratigraphic observation of cyclic deposition of foraminifera-bearing mudstones occurring in both the U1359 and U1361 drill sites, a lithology that is unique in the IODP Expedition 318 drill cores [*Escutia et al.*, 2011]. The top of this interval corresponds with the top of the Jaramillo subchron at both sites. In U1359 the thickness of this interval is 8.55 m, occurring between 33.33 and 24.68 mcd in the composite section from Holes U1359A, B, and C, whereas this distinct interval is 7.1 m thick at U1361. This difference in thickness between sites is consistent with the assumed difference in sedimentation rates derived from higher in the core of ~24 m/m.y. and 18 m/m.y. for U1359 and U1361, respectively. As the base of this foraminifera-bearing interval occurs 6 m below the base of the Cobb Mountain subchron in U1359, it is predicted to occur ~4.5 m below the Cobb Mountain in U1361A owing to the lower sedimentation in that hole. The base of this foraminifera-bearing interval actually occurs 4.1 m below the base of the N3 reversal in U1361 (Figure 15), and is therefore in good agreement with the estimated depth derived above. This supports the interpretation that sedimentation rate is relatively linear, or at

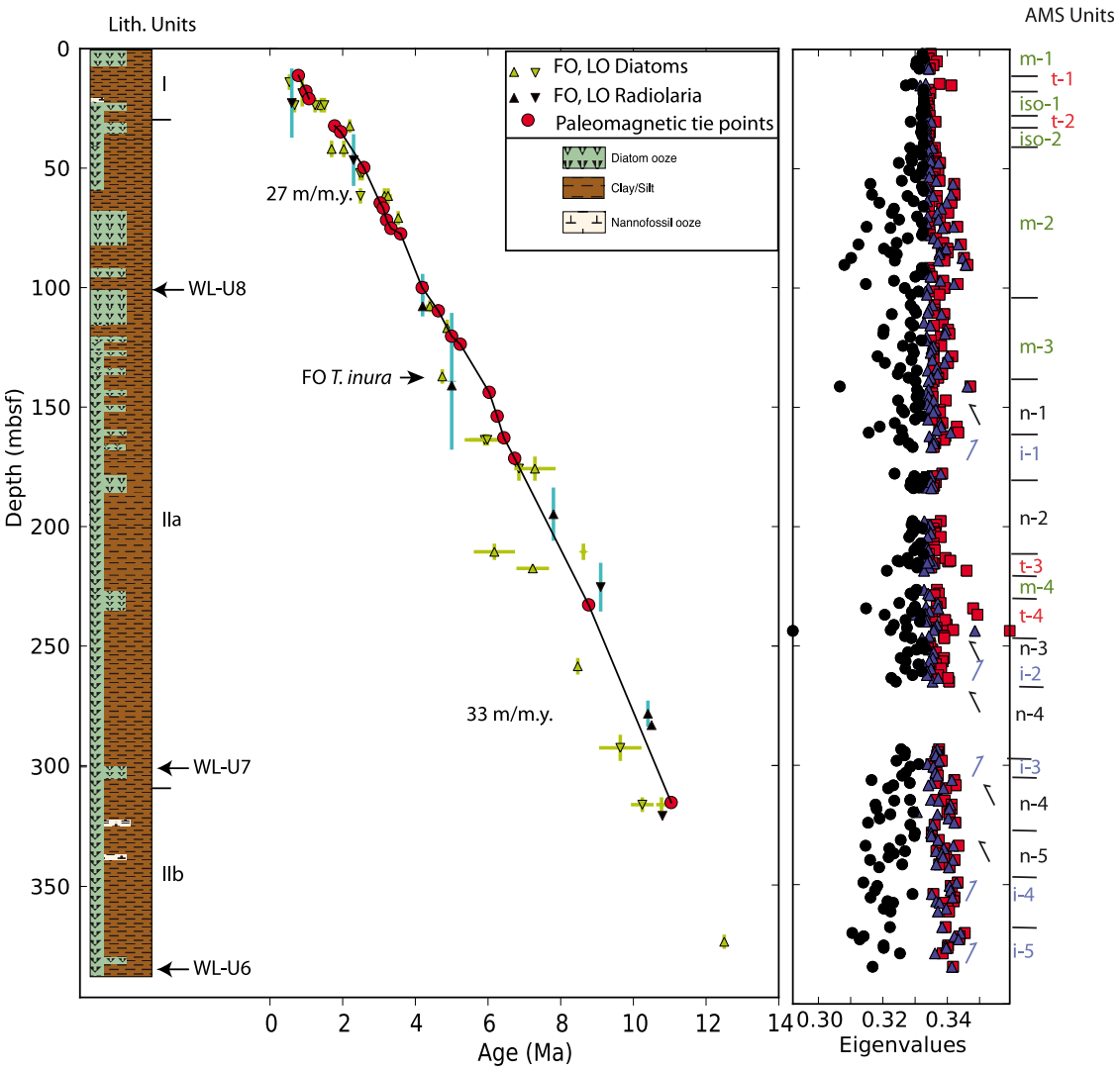

Figure 16. Same as Figure 11, but for U1361A. Paleomagnetic tie points as in Figure 10 and Table S6.

least comparable, between sites and that N3 in U1361 is likely the Cobb Mountain.

[44] Unlike at Site U1359, the Olduvai (Chron C2n) is present, sitting between 32.35 and 34.85 mbsf. However, the four subchrons of the Gilbert (Chron C3n.1n to C3n.4n) are less well expressed. We infer that C3n.1n and C3n.2n are concatenated due to missing material at a core break. Note that the model age for the FO of *T. inura* of *Cody et al.* [2008] is once again discrepant with the magnetostratigraphic interpretation as it was at Site U1359. Chrons C3An and C5n.2n are readily identifiable and the identification of Chron C4A (y) is fairly robust. The interval from C3B to C4, however, appears under-sampled with some of the subchrons being missed. It also appears that the radiolarian events are systematically older than the diatom events in the interval between 200 and 300 mbsf, while the magnetostratigraphic interpretation falls between the two. Overall, sediment accumulation rates were fairly uniform, ranging from ~33 m/m.y. at the bottom of the site to ~27 m/m.y. at the top and there are no major gaps in the record.

4.3.2. Anisotropy of Magnetic Susceptibility

[45] The behavior of AMS at Site U1361 is shown to the right of Figure 16. As at Site U1359, the interval below about 10 Ma, or ~300 mbsf at Site U1361 is characterized by mostly normal AMS trends with a high degree of anisotropy ($P \sim 1.08$). The Pliocene interval is again dominated by mixed intervals with alternations between the diatom-rich (low anisotropy) and diatom-poor (high anisotropy) layers. Unlike Site U1359, however, there are two layers of essentially isotropic fabrics (i-1 and i-2) separated by layers of triaxial fabrics (t-1 and t-2). The latter appears to coincide with the lithologic Unit I/IIa boundary, while the other triaxial horizons are not associated with major lithological boundaries.

4.4. Timing of the Wilkes Land Unconformities

[46] *Escutia et al.* [2011] predicted the depths of three regional unconformities identified in seismic sections on the lithologic log for Site U1356. These are WL-U3, WL-U4 and WL-U5 at 867, 708 and 534 mbsf respectively as shown as black arrows in Figure 11. These have inferred ages of

32.9, 27.0 and 24.3 Ma based on our magnetostratigraphic correlation. WL-U4 is closely associated with the triaxial AMS zones t-4 and a profound change in sediment accumulation rate inferred from the magnetostratigraphic interpretation. The association with triaxial fabrics may not be a coincidence as the triaxial fabrics are a strong indication of disturbed sedimentation. The position of WL-U5 was revised to be at the Unit III/IV boundary (459.4 mbsf) in *Escutia et al.* [2011, Figure F3] and shown as the red arrow in Figure 11 because of the large impedance contrast associated with the lithologic boundary. It is also possible that the nannofossil ooze/clay boundary at the base of Unit III (~440 mbsf) would also provide the impedance contrast necessary to produce the WL-U5 seismic signal. This would be only slightly below the observed hiatus between the top of the Oligocene and the middle Miocene, whose base is just below 432 mbsf. The predicted location of WL-U3 was revised in *Escutia et al.* [2011, Figure F3] to be coincident with Unit IX (879.7895.5 mbsf), described as contorted and convoluted claystones (red arrows in Figure 11). This is only slightly above both the hiatus tied with the lithological boundary between Unist IX and X and AMS triaxial unit t-6.

[47] At Site U1359, the predicted depths of Wilkes Land unconformities WL-U6, WL-U7 and WL-U8 of *Escutia et al.* [2011] are approximately 520, 323, and 126 mcd respectively (Figure 14). Their ages are inferred to be 12.5, 10.5 and 4.9 Ma, based on the magnetostratigraphic correlation shown in the plot. They correspond to the bases of AMS units n-8, i-1 and the top of t-2 respectively. None of these are major unconformities; rather, the stratigraphy itself is continuous but has large changes in sediment accumulation rate. It appears that the degree of AMS anisotropy is quite sensitive to these lithologic changes, which are not as obvious in the lithologic logs themselves.

[48] Finally, the predicted depths of Wilkes Land unconformities WL-U6, WL-U7 and WL-U8 of *Escutia et al.* [2011] are at approximately 385, 300 and 100 mbsf respectively at Site U1361 (Figure 16). Their ages are inferred to be 12.8, 10.6 and 4.2 Ma respectively, based on the magnetostratigraphic correlation shown in the plot. These ages are somewhat different than those inferred for the same horizons at Site U1359. The bottom two are within a few hundred thousand years of each other but WL-U8 differs by about 0.7 Ma. Shifting the horizon down by about 10 m, well within the uncertainty of the placement, would bring it into concordance with the record at Site U1359. Seismic horizon WL-U6 appears to correlate with AMS unit i-5, WL-U7 corresponds to the bases of AMS units i-3, and WL-U8 occurs at the m-2/m-3 boundary.

[49] Expected depths for regional unconformities described on the Eastern Wilkes Land margin by *Escutia et al.* [2011] were calculated using velocity sonobuoy solutions obtained by cruises in the area *Stagg et al.* [2005]. Because the quality of the solutions in some cases is uncertain, one of the aims of the drilling was to calibrate the seismic interpretations by providing the true depths for these unconformities, which could vary as much as 100 m from the predicted depths. Of all unconformities interpreted in the Wilkes Land margin, three of them, WL-U3, WL-U4 and WL-U5, can be traced for long distances, hence are regional in nature. These were interpreted to mark important changes in the development and evolution of the continental East Antarctic Ice Sheet [*Escutia et al.*, 2005, 2011]. Younger unconformities (i.e., WL-U6 to WL-U8), were tentatively traced across large channel-levee systems based on changes in seismic facies [*Donda et al.*, 2003]. Therefore it is not surprising that they do not represent major unconformities and that the ages for the interpreted unconformities may be somewhat different in Sites 1359 and Site 1361.

5. Conclusions

[50] Paleoceanographic reconstructions from Wilkes Land margin drill cores critically depend on a robust stratigraphic framework. Paleomagnetic data derived from measurement of the archive halves on board the JOIDES Resolution and discrete samples in the paleomagnetic laboratory at Scripps Institution of Oceanography satisfy minimum requirements for a reliable magnetostratigraphic record. Although recovery was discontinuous and much of the core material was disturbed either by the coring process or by slumping or other depositional processes, we were able to tie many of the reversal boundaries to the geomagnetic polarity timescale. Most of our interpretations are consistent with the available biostratigraphic events [from *Escutia et al.* [2011]; this study].

[51] Here we summarize the chronostratigraphic data available at this time. This paper improves on earlier work *Escutia et al.* [2011] and moves toward excellent stratigraphic control in order to better understand the timing of key paleoclimatic events for critical climate intervals for this important region. The evidence presented in this paper provides the opportunity for improved chronostratigraphic calibration. The current age calibrations of several diatom events in the Pliocene appear to be "too young". As these were calibrated in sequences with less robust magnetostratigraphic data, we suggest that the calibration put forward in this paper be used in constructing future age models. Also, there appears to be a distinct offset between the radiolarian and diatom chronologies in the Miocene. Finally, magnetostratigraphic calibration of dinocysts in the Southern Ocean has been problematic and the data from Hole U1356A provide the opportunity significantly improve the FO and LO ages for these biostratigraphic indicators in the middle Oligocene and middle Eocene.

[52] The data provided in this paper contribute to the recognition and age calibrations for the Wilkes Land regional seismic horizons (the "regional unconformities" of *Escutia et al.* [2011]) WL-U3 to WL-U8. While WL-U3 does appear to be a massive unconformity most likely corresponding to the hiatus between the middle Eocene and the lowermost Oligocene, the others are not. WL-U4 occurs near an abrupt change in sediment accumulation rate (not an unconformity) and is here dated at ~27 Ma while WL-U5 is dated at 24.3 Ma. WL-U6, WL-U7 and WL-U8 were cored in both U1359 and U1361. Age estimates for the first two agreed reasonably well (WL-U6: 12.5 and 12.8 Ma, respectively, and WL-U7: 10.5 and 10.6 Ma, respectively) but the estimates for WL-U8 were somewhat different (4.9 and 4.2 Ma respectively). The age estimates can be brought into accord by shifting the WL-U8 horizon downward by ~10 m in U1361 from its originally predicted depth.

[53] The stratigraphic framework developed here allows the placement of future proxy-based paleo-records into a

context of global climate and ocean circulation models during a critical period of time. The record from the Wilkes Land Margin will contribute significantly to our understanding of Antarctic climate and ice sheet evolution and their feedbacks to the global climate system.

[54] **Acknowledgments.** We are deeply grateful for the hard work of the entire shipboard party of IODP Expedition 318, including scientific, technical, and support staff. In particular, we wish to thank Maggie Hastedt, whose tireless and cheerful help in the paleomagnetic laboratory was essential to the success of our investigations. We thank Joe Smoot, Jan Backman, two anonymous reviewers, and the Editor, Rainer Zahn, for careful review which greatly improved the manuscript. This research used samples and data provided by the Integrated Ocean Drilling Program (IODP). Funding for this research was provided by NSF grants OCE1058858 and OCE1054497 to L.T.

References

Acton, G., M. Okada, B. M. Clement, S. Lund, and T. Williams (2002), Paleomagnetic overprints in ocean sediment cores and their relationship to shear deformation caused by piston coring, *J. Geophys. Res.*, *107*(B4), 2067, doi:10.1029/2001JB000518.

Agnini, C., G. Muttoni, D. V. Kent, and D. Rio (2006), Eocene biostratigraphy and magnetic stratigraphy from Possagno, Italy: The calcareous nannofossil response to climate variability, *Earth Planet. Sci. Lett.*, *241*, 815–830, doi:10.1016/j.epsl.2005.11.005.

Bijl, P. K. (2011), Environmental and climatological evolution of the early Paleogene Southern Ocean, PhD thesis, Utrecht Univ., Utrecht, Netherlands.

Bijl, P. K., A. J. P. Houben, S. Schouten, S. Bohaty, A. Sluijs, G.-J. Reichart, J. S. Sinninghe Damsté, and H. Brinkhuis (2010), Transient Middle Eocene atmospheric CO_2 and temperature variations, *Science*, *330*, 819–821, doi:10.1126/science.1193654.

Bohaty, S. M., J. C. Zachos, and M. L. Delaney (2012), Foraminiferal Mg/Ca evidence for Southern Ocean cooling across the Eocene-Oligocene transition, *Earth Planet. Sci. Lett.*, *317–318*, 251–261, doi:10.1016/j.epsl.2011.11.037.

Channell, J. E. T., and J. S. Stoner (2002), Plio-Pleistocene magnetic polarity stratigraphies and diagenetic magnetite dissolution at ODP Leg 177 Sites (1089, 1091, 1093, and 1094), *Mar. Micropaleontol.*, *45*, 269–290, doi:10.1016/S0377-8398(02)00032-4.

Channell, J. E. T., D. A. Hodell, C. Xuan, A. Mazaud, and J. S. Stoner (2008), Age calibrated relative paleointensity for the last 1.5 Myr at IODP Site U1308 (North Atlantic), *Earth Planet. Sci. Lett.*, *274*, 59–71, doi:10.1016/j.epsl.2008.07.005.

Cody, R. D., R. H. Levy, D. M. Harwood, and P. M. Sadler (2008), Thinking outside the zone: High-resolution quantitative diatom biochronology for the Antarctic Neogene, *Palaeogeogr., Palaeoclimatol., Palaeoecol.*, *260*, 92–121, doi:10.1016/j.palaeo.2007.08.020.

Constable, C., and L. Tauxe (1990), The bootstrap for magnetic susceptibility tensors, *J. Geophys. Res.*, *95*, 8383–8395, doi:10.1029/JB095iB06p08383.

Crouch, E. M., and H. Brinkhuis (2005), Environmental change across the Paleocene-Eocene transition from eastern New Zealand: A marine palynological approach, *Mar. Micropaleontol.*, *56*, 138–160, doi:10.1016/j.marmicro.2005.05.002.

Donda, F., G. Brancolini, L. De Santis, and F. Trincardi (2003), Seismic facies and sedimentary processes on the continental rise off Wilkes Land (East Antarctica): Evidence of bottom current activity, *Deep Sea Res., Part II*, *50*, 1509–1527, doi:10.1016/S0967-0645(03)00075-4.

Escutia, C., L. De Santis, F. Donda, R. B. Dunbar, A. K. Cooper, G. Brancolini, and S. L. Eittreim (2005), Cenozoic ice sheet history from East Antarctic Wilkes Land Continental Margin sediments, *Global Planet. Change*, *45*, 51–81, doi:10.1016/j.gloplacha.2004.09.010.

Escutia, C., H. Brinkhuis, A. Klaus, and Expedition 318 Scientists (2011), *Wilkes Land Glacial History*, *Proc. Integr. Ocean Drill. Program*, *318*.

Fioroni, C., G. Villa, D. Persico, S. W. Wise, and L. Pea (2012), Revised middle Eocene-upper Oligocene calcareous nannofossil biozonation for the Southern Ocean, *Rev. Micropaleontol.*, doi:10.1016/j.revmic.2012.03.001, in press.

Fisher, N. I., T. Lewis, and B. J. J. Embleton (1987), *Statistical Analysis of Spherical Data*, Cambridge Univ. Press, Cambridge, U. K.

Fisher, R. A. (1953), Dispersion on a sphere, *Proc. R. Soc. London, Ser. A*, *217*, 295–305, doi:10.1098/rspa.1953.0064.

Florindo, F., and A. P. Roberts (2005), Eocene-Oligocene magnetobiochronology of ODP Sites 689 and 690, Maud Rise, Weddell Sea, Antarctica, *Geol. Soc. Am. Bull.*, *117*, 46–66, doi:10.1130/B25541.1.

Fuller, M., and Y. Touchard (2004), On the magnetostratigraphy of the East Tasman Plateau Timing of the opening of the Tasmanian Gateway and paleoenvironmental changes, in *The Cenozoic Southern Ocean: Tectonics, Sedimentation, and Climate Change Between Australia and Antarctica*, *Geophys. Monogr. Ser.*, vol. 151, edited by N. F. Exon, J. P. Kennett, and M. J. Malone, pp. 63–78, AGU, Washington, D. C., doi:10.1029/151GM05.

Gee, J. S., L. Tauxe, and C. Constable (2008), AMSSpin: A LabVIEW program for measuring the anisotropy of magnetic susceptibility with the Kappabridge KLY-4S, *Geochem. Geophys. Geosyst.*, *9*, Q08Y02, doi:10.1029/2008GC001976.

Gradstein, F. M., J. G. Ogg, and A. G. Smith (2004), *Geologic Time Scale 2004*, Cambridge Univ. Press, Cambridge, U. K.

Hollis, C. J., et al. (2009), Tropical sea temperatures in the high-latitude South Pacific during the Eocene, *Geology*, *37*, 99–102, doi:10.1130/G25200A.1.

Houben, A. J. P., P. K. Bijl, G. R. Guerstein, A. Sluijs, and H. Brinkhuis (2011), Malvinia escutiana, a new biostratigraphically important Oligocene dinoflagellate cyst from the Southern Ocean, *Rev. Palaeobot. Palynol.*, *165*, 175–182, doi:10.1016/j.revpalbo.2011.03.002.

Iwai, M., G. Acton, D. Lazarus, L. E. Osterman, and T. Williams (2002), Magnetobiochronologic synthesis of ODP Leg 178 rise sediments from the Pacific sector of the Southern Ocean: Sites 1095, 1096, and 1101, *Proc. Ocean Drill. Program Sci. Results*, *178*, doi:10.2973/odp.proc.sr.178.236.2002.

Kirschvink, J. L. (1980), The least-squares line and plane and the analysis of paleomagnetic data, *Geophys. J. R. Astron. Soc.*, *62*, 699–718, doi:10.1111/j.1365-246X.1980.tb02601.x.

Miller, K. G., J. D. Wright, and R. G. Fairbanks (1991), Unlocking the Ice House: Oligocene-Miocene oxygen isotopes, eustasy and margin erosion, *J. Geophys. Res.*, *96*, 6829–6848, doi:10.1029/90JB02015.

Parker, R. L. (2000), Calibration of the pass-through magnetometer—I. Theory, *Geophys. J. Int.*, *142*, 371–383, doi:10.1046/j.1365-246x.2000.00171.x.

Parker, R. L., and J. S. Gee (2002), Calibration of pass-through magnetometer—II. Application, *Geophys. J. Int.*, *150*, 140–152, doi:10.1046/j.1365-246X.2002.01692.x.

Payros, A., J. Dinarès-Turell, G. Bernaola, X. Orue-Etxebarria, E. Apellaniz, and J. Tosquella (2011), On the age of the Early/Middle Eocene boundary and other related events: cyclostratigraphic refinements from the Pyrenean Otsakar section and the Lutetian GSSP, *Geol. Mag.*, *148*, 442–460, doi:10.1017/S0016756810000890.

Percival, S. F., Jr. (1984), Late Cretaceous to Pleistocene calcareous nannofossils from the South Atlantic, DSDP Leg 73, *Initial Rep. Deep Sea Drill. Proj.*, *73*, 391–424, doi:10.2973/dsdp.proc.73.109.1984.

Pross, J., et al. (2012), Persistent near-tropical warmth on the Antarctic continent during the early Eocene epoch, *Nature*, in press.

Roberts, A. P., S. J. Bicknell, J. Byatt, S. M. Bohaty, F. Florindo, and D. M. Harwood (2003), Magnetostratigraphic calibration of Southern Ocean diatom datums from the Eocene-Oligocene of Kerguelen Plateau (Ocean Drilling Program sites 744 and 748), *Palaeogeogr., Palaeoclimatol., Palaeoecol.*, *198*, 145–168, doi:10.1016/S0031-0182(03)00397-3.

Sakai, H., and B. H. Keating (1991), Paleomangetism of Leg 119–Holes 737A, 738 C, 742A, 745B, 746A, *Proc. Ocean Drill. Program Sci. Results*, *119*, 751–770, doi:10.2973/odp.proc.sr.119.150.1991.

Schwehr, K., L. Tauxe, N. Driscoll, and H. Lee (2006), Detecting compaction disequilibrium with anisotropy of magnetic susceptibility, *Geochem. Geophys. Geosyst.*, *7*, Q11002, doi:10.1029/2006GC001378.

Shackleton, N. J., M. A. Hall, I. Raffi, L. Tauxe, and J. Zachos (2000), Astronomical calibration age for the Oligocene-Miocene boundary, *Geology*, *28*, 447–450, doi:10.1130/0091-7613(2000)28<447:ACAFTO>2.0.CO;2.

Spieß, V. (1990), Cenozoic magnetostratigraphy of Leg 113 drill sites, Maud Rise, Weddell Sea, Antarctica, *Proc. Ocean Drill. Program Sci. Results*, *113*, 261–315, doi:10.2973/odp.proc.sr.113.182.1990.

Stagg, H. M. J., J. B. Colwell, N. G. Direen, P. E. O'Brien, B. J. Brown, G. Bernardel, I. Borissova, L. Carson, and D. B. Close (2005), Geological framework of the continental margin in the region of the Australian Antarctic Territory, *Geosci. Aust. Rec. 2004/25*, 373 pp., Geosci. Aust., Canberra.

Steininger, F. F., et al. (1997), The Global Stratotype Section and Point (GSSP) for the base of the Neogene, *Episodes*, *20*, 23–28.

Tauxe, L., P. Tucker, N. Petersen, and J. LaBrecque (1983), The magnetostratigraphy of Leg 73 sediments, *Palaeogeogr. Palaeoclimat. Palaeoecol.*, *42*, 65–90, doi:10.1016/0031-0182(83)90039-1.

Tauxe, L., R. Butler, R. van der Voo, and S. K. Banerjee (2010), *Essentials of Paleomagnetism*, Univ. of Calif. Press, Berkeley.

Wei, W., K. L. McGonigal, and S. Zhong (2004), Data report: Paleogene calcareous nannofossil biostratigraphy of ODP Leg 189 (Australia-